https://doi.org/10.5194/essd-2026-718
Preprint. Discussion started: 21 September 2026

Open Access Earth System Science Data Discussions

Seasonal evolution of a warm alpine snowpack: a multi-instrument dataset of snow microstructure at Col de Porte, French Alps

Neige Calonne[1], Pascal Hagenmuller[1], Rémi Granger[1], Lisa Bouvet[1], Kévin Fourteau[1], Julien Brondex[1], François Tuzet[1], Yves Lejeune[1], Anne Dufour[1], Mathieu Fructus[1], Teruo Aoki[2], and Marie Dumont[1]

[1]Météo-France, CNRS, Univ. Grenoble Alpes, Univ. Toulouse, CNRM, Centre d'Études de la Neige, 38000 Grenoble, France
[2]Meteorological Research Institute, Tsukuba, Japan

Correspondence: Neige Calonne (neige.calonne@meteo.fr) and Marie Dumont (marie.dumont@meteo.fr)

Abstract.

Long-term snow observation sites provide valuable datasets for understanding snowpack evolution and evaluating snow models. Recent observation campaigns have progressively enriched these monitoring programs with high-resolution measurements of snow microstructure, particularly using the SnowMicroPen. Here, we present a two-winter dataset of snow and atmospheric observations collected at Col de Porte (French Alps, 1325 m), a warm alpine environment, during the winters 2021–2022 and 2022–2023. The dataset extends the standard observation program with weekly vertical profiles of snow density, specific surface area (SSA), structural anisotropy, and penetration resistance obtained from the SnowMicroPen, X-ray tomography, density cutters, and two optical reflectance instruments (DUFISSS and HISSGraS). Tomography measurements combined fast acquisitions (42 µm) and high-resolution acquisitions (10 µm). The study (i) provides a comprehensive dataset of snow microstructural properties together with atmospheric forcing for snow model evaluation under warm snow conditions, characterized by frequent wet snow and melt-freeze crusts, and (ii) assesses the strengths and limitations of the different measurement techniques, including the feasibility of seasonal snowpack monitoring by X-ray tomography, the use of the SnowMicroPen under warm snow conditions, and the agreement between the two optical reflectance instruments. The paper describes the meteorological and snowpack conditions during the two winters, presents multi-instrument vertical profiles of snow density and SSA, and reports the characteristic ranges of density, SSA, and structural anisotropy for the different snow types encountered at Col de Porte. The dataset is available at https://doi.org/10.6084/m9.figshare.33426472 (Calonne et al., 2026).

1 Introduction

In situ snow observations are crucial for understanding snow properties, snow evolution, and the physical processes responsible for this evolution (Krinner et al., 2018). They are essential to many applications, such as climate trend studies (e.g. Dumont et al., 2025), remote sensing data analysis (e.g. Lemmetyinen et al., 2018), snow model evaluation (e.g. Essery et al., 2013), or avalanche and water resource forecasting (Bader, 1939). Standard snow observations generally include measurements of snow bulk properties, such as snow height or snow water equivalent, and, sometimes, measurements of the snowpack stratigraphy, such as the vertical profile of density, specific surface area (SSA), visual grain types and sizes, hardness, temperature, and liquid

https://doi.org/10.5194/essd-2026-718
Preprint. Discussion started: 21 September 2026

water content (e.g. Fierz et al., 2009; Ménard et al., 2019). A variety of field instruments are classically used to retrieve these snow properties, from traditional ones, such as density cutters, Ramsonde, and magnifying glass, to more modern ones, such as optical reflectance instruments (e.g. Gallet et al., 2009) and snow micro-penetrometers (SMP) (Schneebeli et al., 1999). Recently, a few observation campaigns started to use X-ray tomography for in-situ snowpack monitoring (Calonne et al., 2020; Macfarlane et al., 2023), previously restricted to snow studies in a cold laboratory. Tomography gives access to a three-dimensional (3D) image of the snow microstructure at the micron scale, and thus, to the microstructural properties of snow (e.g. Coléou et al., 2001; Calonne et al., 2014; Krol and Löwe, 2016). From these images, the effective properties of snow, such as albedo (Robledano et al., 2023), thermal conductivity (Calonne et al., 2011; Löwe et al., 2013), or different mechanical properties (Schleef and Loewe, 2013; Védrine et al., 2024) can be simulated.

All over the world, snow observation sites are maintained and provide winter-long time series of snow properties. Among these sites, Sodankyla in Finland (Essery et al., 2016), Col de Porte in France (Morin et al., 2012; Lejeune et al., 2019), and Weissfluhjoch in Switzerland (Marty and Meister, 2012; Calonne et al., 2020; Löwe et al., 2025) provide essential snow measurements over more than half a century. At these sites, both snow and atmospheric properties are monitored, offering datasets for driving and evaluating the snow models. The first seasonal snow dataset that includes snow microstructure properties from tomography and from SMP measurements was obtained at Weissfluhjoch, a high-elevation site located at an altitude of 2536 m, by Calonne et al. (2020). With SMP measurements performed daily, they showed the benefits of high-resolution data of density and SSA for snow model evaluation.

The objective of the present paper is to provide and describe a two-year dataset of snow and meteorological observations at Col de Porte (1325 m a.s.l, French Alps), which includes detailed weekly measurements of the vertical profile of snow properties (traditional snow profile, X-ray imaging, density, and SSA). The goal was i) to obtain a dataset for driving and evaluating snow models at a 'warm' alpine site, and ii) to explore our ability to integrate tomographic measurements into the weekly standard observations, for the monitoring of snow microstructure at high resolution. For those purposes, during winter 2021–2022 and 2022–2023, the standard observation program of the Col de Porte site (Lejeune et al., 2019), a mid-elevation site located at 1325 m, was complemented by additional weekly measurements of highly-resolved vertical profiles of density and specific surface area by tomography, SMP, density cutter, and two optical reflectance devices: DUFISSS (Gallet et al., 2009) and HISSGraS (Aoki et al., 2023). Two methods of tomography were tested, allowing different image resolutions and scan durations: the high-resolution scan method at 10 µm and the fast scan method at 42 µm. This specific campaign is referred to as the IVORI campaign at Col de Porte, as part of the ERC IVORI project.

The paper first describes the measurement campaign, the instruments, and the processing methods. Next, we describe the atmospheric and snowpack conditions during the two winter seasons, which are put into perspective with the climatological records. Then, we present our dataset of density and SSA vertical profiles and discuss its potential for snow model evaluation through layer tracking. The usage and performance of the instruments and methods of the field campaign are commented on, notably SMP measurements in 'warm' snowpack.

https://doi.org/10.5194/essd-2026-718
Preprint. Discussion started: 21 September 2026

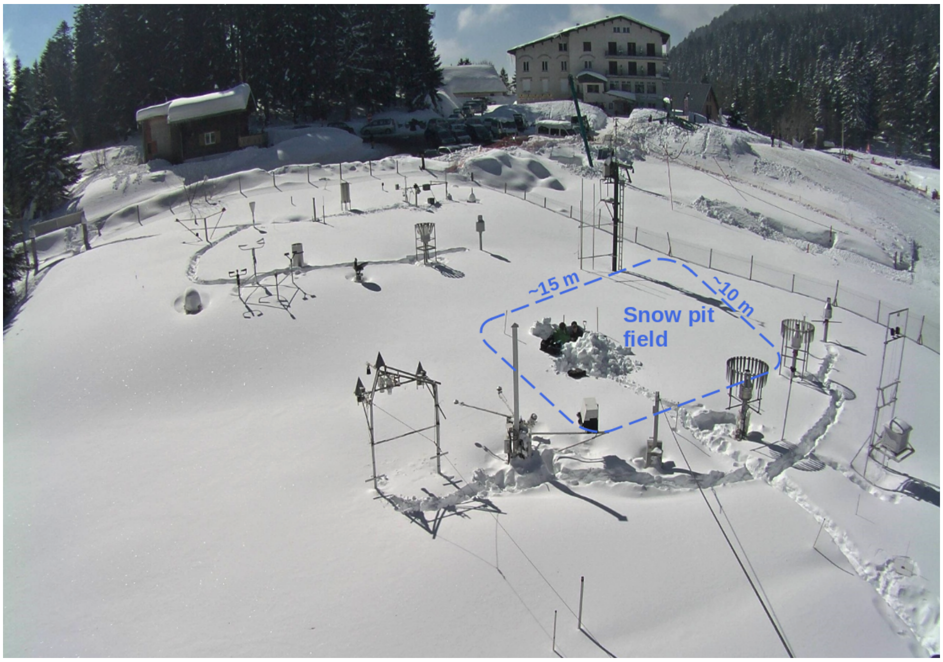

Figure 1. Picture of the observation field site for automatic and manual measurements at Col de Porte (credit: Y. Lejeune, CNRM). The snow pit field, in which the IVORI measurements were done, is shown.

2 The IVORI measurement campaigns at Col de Porte

2.1 The Col de Porte observation site

Our measurement campaigns were carried out at Col de Porte (45.30° N, 5.77° E), a site dedicated to the study and monitoring of the meteorology and snow since 1959 (Lejeune et al., 2019). Col de Porte is located at an elevation of 1325 m in the northwestern part of the French Alps, on the border of the main Alpine range, near Grenoble, France. The study field of Col de Porte corresponds to a flat to low-slope grassy meadow surrounded by pine trees, as illustrated with the overview picture in Figure 1. The site exhibits the characteristics of a low-elevation alpine snowpack environment, characterized by relatively warm and wet conditions. Over the period 1990–2020, from November 1 to April 30, the site shows a mean snowpack height of 53 cm, a mean air temperature of 1.15°C, and a mean total precipitation (rain and snow) of 989 kg m^{-2} (Lejeune et al., 2019; Dumont et al., 2025). In comparison, the Weissfluhjoch site, located at 2536 m of elevation and located in the inner part of the Eastern Swiss Alps, shows a much higher mean snow height of 142 cm combined with a much lower mean air temperature of -6.37°C and lower mean total precipitation of 555 kg m^{-2}, over the same period (Dumont et al., 2025). The impact of climate change at Col de Porte is very pronounced. The mean snow height decreased by about -32.7 cm between the periods 1960–1990 and 1990–2020 (corresponding to a 39% decrease). Over the same periods, the snow cover duration has shortened by 22 days on average, associated with an increase in air temperature of +1.01°C and no significant change in total

https://doi.org/10.5194/essd-2026-718
Preprint. Discussion started: 21 September 2026

Open Access Earth System Science Data Discussions

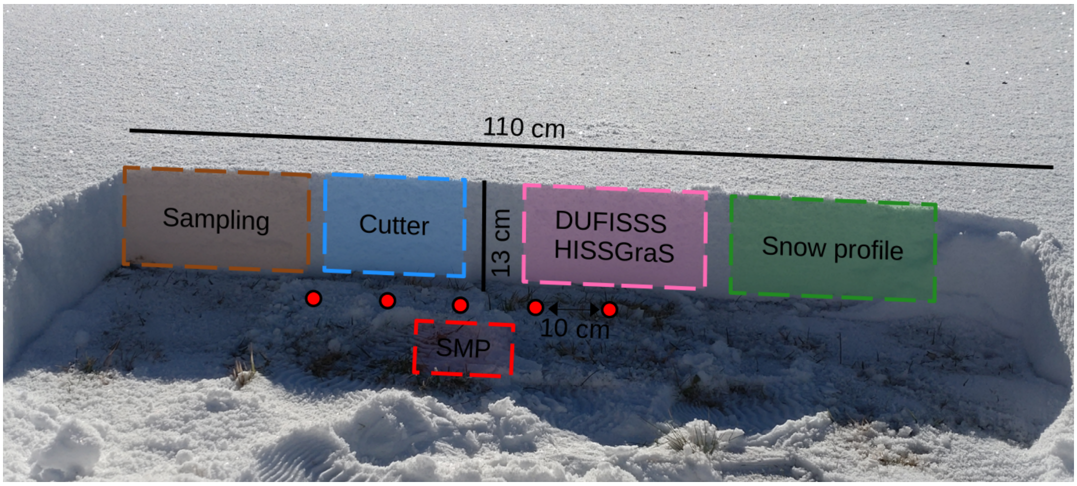

Figure 2. Schematic of the organization of the measurements in the snow pit, illustrated for January 10, 2023 (credit: N. Calonne). The SMP measurements were performed before digging the snow pit and are represented here a few cm in front of the pit wall.

precipitation (a decrease of -17 kg m^{-2} corresponding to 1.7%). The primary reason for the increased snow scarcity at low and mid-elevations, such as the Col de Porte site, is the shift in precipitation phase, i.e., more rain and less snow Hock et al. (2019); Dumont et al. (2025).

At Col de Porte, automatic hourly measurements include air and soil temperatures, wind speed and direction, air pressure and humidity, precipitation, shortwave and longwave incident radiation, outgoing longwave radiation, reflected shortwave radiation, snow surface temperature, and total snow height. Manual weekly measurements are also performed and include total snow water equivalent, snow water equivalent of fresh snow, and the standard snow profiling (temperature profile, Ramsonde hardness profile, layer hand hardness, layer grain type and size, layer density, and layer liquid water content). These automatic and manual measurements constitute the standard observation program at Col de Porte, as carried out every winter. They are detailed in Lejeune et al. (2019) and the dataset of the snow and atmospheric properties is available in the repository https://doi.org/10.17178/CRYOBSCLIM.CDP.2018.

2.2 Overview and sequence of measurements

During the winters of 2021–2022 and 2022–2023, the standard weekly observations at Col de Porte were supplemented by additional measurements of vertical snow property profiles. These measurements are synthesized in Table 1. The first campaign ran from November 30, 2021, to April 12, 2022, and the second one ran from January 10, 2023, to March 28, 2023. We recorded vertical profiles of density by cutter measurements, vertical profiles of SSA with two optical instruments (DUFISSS and HISSGraS), vertical profiles of penetration force with the penetrometer SnowMicroPen (SMP), and vertical profiles of the snow microstructure by tomography measurements, following a high-resolution (HR) method and a fast scanning (LR) method. The methods and data processing applied for each instrument are described later in this section. These measurements

https://doi.org/10.5194/essd-2026-718
Preprint. Discussion started: 21 September 2026

Open Access Earth System Science Data Discussions

were performed in the field reserved for the snow pits and manual snow measurements, indicated by the blue rectangle in Figure 1. The profiles cover the entire height of the snowpack, except for the tomography measurements that cover only part of it. They show a vertical resolution ranging from 10 microns to 3 cm, depending on the instrument (Tab. 1). The measurements were performed weekly, with a few exceptions. Dates for each measurement are provided in Figure 3. No measurements were taken with the SMP from mid-January to mid-February 2022, as the instrument was under repair. These additional measurements were not necessarily taken on the same date as the standard Col de Porte observations, as shown in Fig. 3.

The measurements were taken in the field in the following sequence. The organization of the measurements in the snow pit is illustrated in Figure 2 for the date of January 10, 2023. Measurements were taken at a distance of 1 m from the previous measurements, moving in a straight line along corridors defined in the snow study field. All instruments and tools were thermalized outside before use. First, 5 SMP profile measurements spaced 10 cm apart were recorded, following a straight line. Then, the snow pit was dug so that the face of the wall was aligned with the line of the 5 SMP measurements and a few cm past them. The pit wall was about 1 to 1.5 m wide and was divided into several zones, dedicated to the different types of measurements. The snow samples for tomography were taken from the snow pit wall, and the tomographies were carried out in the cold laboratory shortly after. At the same time, the snow pit measurements were performed by another team, which included measurements with the density cutter, DUFISSS, and, at times, HISSGraS. When recorded on the same day, the snow profile was taken in the same snow pit as the other measurements, following the standard methodology described in Fierz et al. (2009). Throughout the paper, the standard snow-type abbreviations used in snow profiles are: PP for precipitation particles, DF for decomposing and fragmented precipitation particles, RG for rounded grains, FC for faceted crystals, DH for depth hoar, SH for surface hoar, MF for melt forms, and IF for ice formations (Fierz et al., 2009). At the end of the measurements, the snow pit was filled with snow, and its position was marked with a pole.

Table 1. Overview of the measurements of the IVORI campaign at Col de Porte

Instrument	Vertical resolution	Derived parameters
HR scan	10 µm (only parts of the snowpack)	Density, SSA, and structural anisotropy computed from the binary 3D snow images
LR scan	42 µm	Same as HR scan, with corrected chord length distributions
SMP	0.5 mm	Density and SSA derived from penetration resistance force
Density cutter	30 mm	Density
DUFISSS	30 mm (3 days at 10 mm)	SSA derived from reflectance
HISSGraS	30 mm (1 day at 10 mm)	SSA derived from reflectance
Snow profile	Layer scale	Grain shape and size, hand hardness, liquid water content, temperature, ram resistance

https://doi.org/10.5194/essd-2026-718
Preprint. Discussion started: 21 September 2026

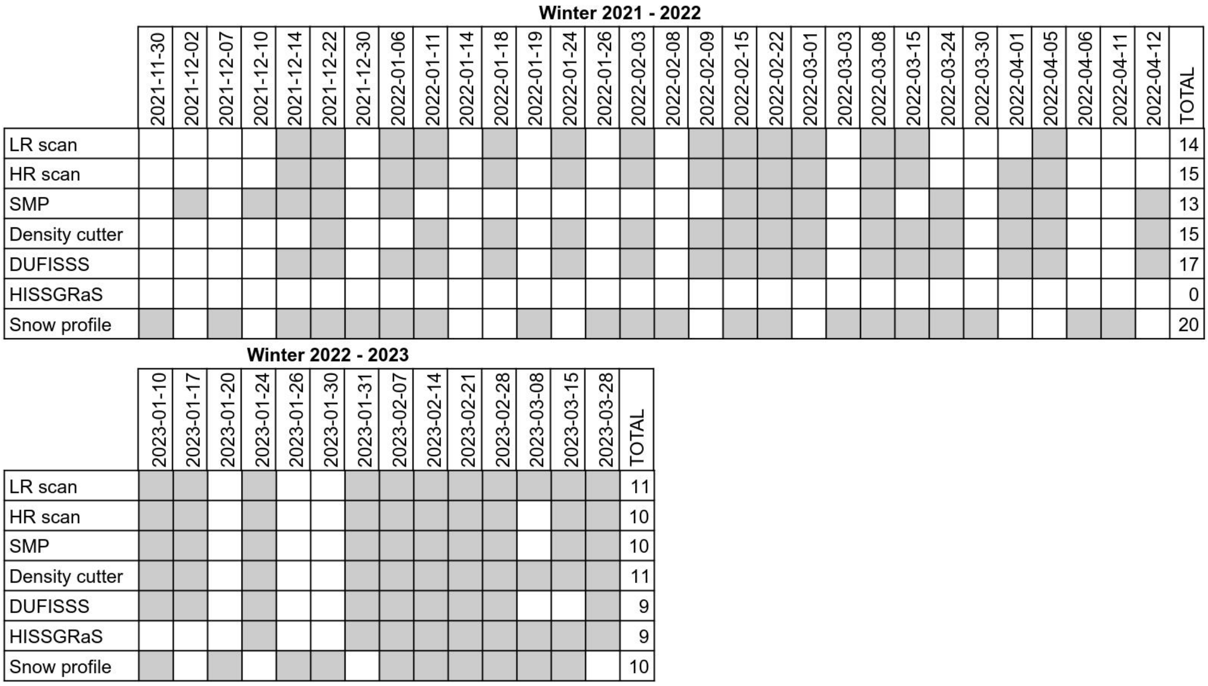

Figure 3. Dates of the measurements performed during the IVORI field campaigns in winter 2021–2022 and 2022–2023.

2.3 Tomography measurements

X-ray tomography was performed to measure the 3D arrangement of air and ice of a snow sample at micrometric resolution (Coléou et al., 2001) and retrieve a high-resolution vertical profile of snow microstructural properties, focused here on density, SSA, structural anisotropy and snow type.

2.3.1 Snow sampling

After digging the snow pit, snow samples were collected for tomography (Fig. 4). An overview of the tools used for snow sampling is presented in Figure 4.b. In the standard procedure, a transparent PMMA cylinder of 4 cm in inner diameter and 10 cm height, referred to as S00 in Figure 4.b, was used for sampling. The end of the cylinder was chamfered to facilitate insertion. The standard sampling procedure was as follows:

- A clean horizontal surface was excavated at the desired height corresponding to the top of the sample.
- The plate of a trowel was inserted at the height corresponding to the bottom of the sample, most of the time 10 to 15 cm below the excavated surface.
- A plastic transparent cylinder of 4 cm in inner diameter was placed on the excavated surface and gently pushed downward until it reached the plate of the trowel, so that the disturbance of the snow microstructure was kept as small as possible.

https://doi.org/10.5194/essd-2026-718
Preprint. Discussion started: 21 September 2026

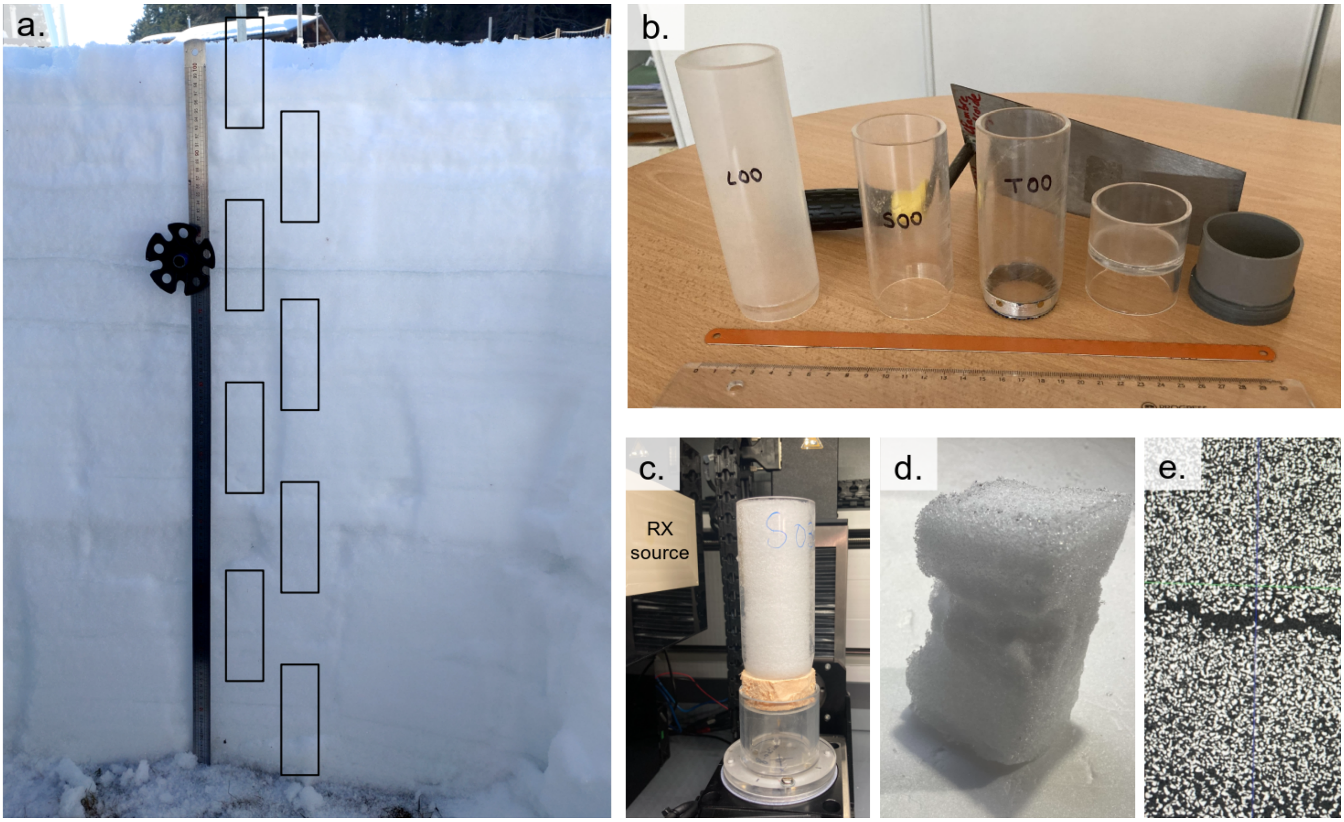

Figure 4. Snow sampling for tomography. a) Overlapping snow sampling location along the snow pit wall, for 8 March, 2022. b) Tools for snow sampling: different types of cylinders, with and without metallic teeth, trowel, metal saw, and bottom plugs to hold the sample in the tomograph (not always used). c) Snow sample in the tomograph in the LR scan position. d) Parallelepiped snow volume cut with the metal saw, before being placed into a cylindrical holder. e) 2D vertical grayscale slice from an LR scan of a snow sample whose sampling failed. A large crack is seen in the middle (white color corresponds to ice, and black color corresponds to air).

- The heights at which the snow sample was extracted from the snowpack were recorded for further vertical referencing.
- The cylinder was then carefully extracted from the snow wall and sealed at the top and bottom with polystyrene caps.
- Finally, the snow sample was transported on foot to the -8°C cold laboratory, located 50 m away from the sampling area. After being thermalized for 30 minutes to 1 hour, the sample was placed into the tomograph installed in the cold laboratory and scanned (Fig. 4.c).
- The same procedure was repeated at the next desired height. An overlap in sample height was made when we wanted to ensure continuity between samples, as illustrated in Fig. 4.a.

Sampling was sometimes challenging. The quality of the sampling was checked on the reconstructed LR scans. An example is given in Figure 4.e, where a large crack in the middle of the image is visible. Difficulties were found for hard layers, typically

https://doi.org/10.5194/essd-2026-718
Preprint. Discussion started: 21 September 2026

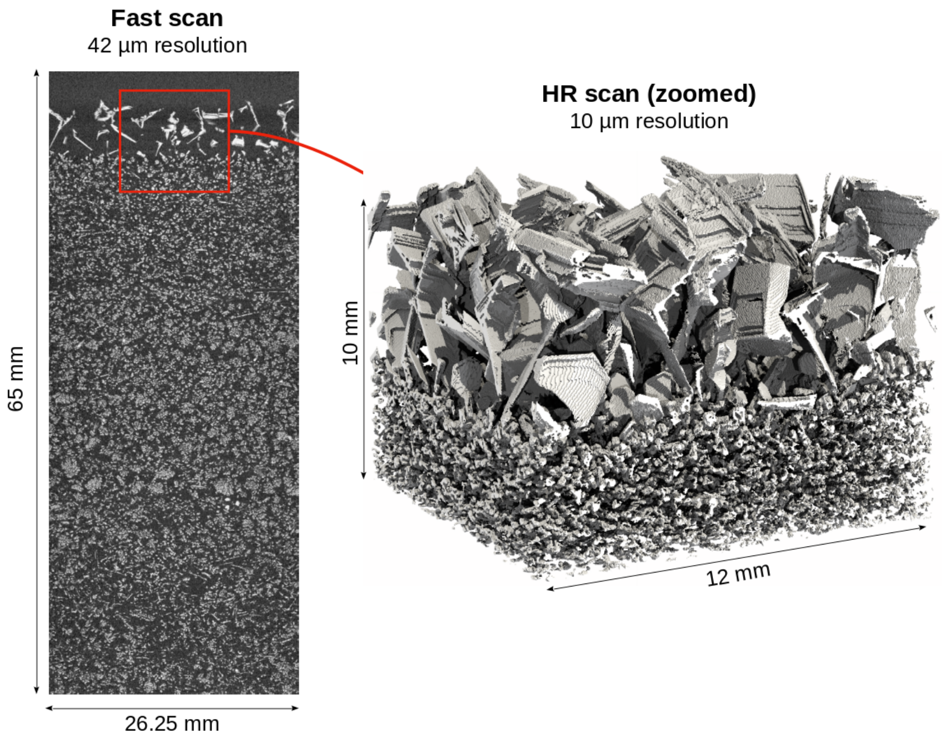

Figure 5. Example of an LR and HR scan from the tomography measurements. Left: 2D vertical grayscale slice from a fast LR scan of the entire snow sample. The white color corresponds to ice, and the black color corresponds to air. Right: 3D segmented image from an HR scan of a sub-volume of the snow sample. The red box indicates the position of the HR scan relative to the LR scan position.

the melt-freeze crusts or ice layers, for which it was not possible to push the cylinder through without damage. In that case, a parallelepiped snow sample was cut with a thin metal saw, as exemplified in Figure 4.d, and then placed in a cylinder for tomography. Note that a sampling cylinder with teeth, referred to as T00 in Figure 4.b, was also tried out on hard layers, inserting the cylinder by smooth rotational movements. It did not provide satisfactory results. Sampling could also be difficult in fresh, light snow, which tended to compact when the cylinder was inserted. This could be detected in the field by checking whether the surface of the snow sample in the cylinder had sunk relative to the surrounding untouched snow surface. Finally, sampling in wet snow was carried out as in dry snow, and the sample was refrozen when placed in the cold laboratory before scanning. In any case, the sampling was repeated until satisfactory. In only a few cases, we did not succeed in sampling, so no tomography data could be obtained.

2.3.2 Tomography acquisitions

Tomography acquisitions were performed with a tomograph RX-Solutions DeskTom (Hagenmuller, 2019). It is composed of a reflection source (Hamamatsu, L9181-02, 130 kV) with a tungsten anode and a flat panel detector (Varian, DX2520) of 1920×1536 pixels with a pitch of 127 µm.

https://doi.org/10.5194/essd-2026-718
Preprint. Discussion started: 21 September 2026

Table 2. Tomography acquisition parameters used for the HR and LR scans.

Parameters	HR scan	LR scan
Voxel size	10 µm	42 µm
Duration	50 min per scan	1 min for 5 mm of snow height
Final image width	12.5 mm (1250 voxels)	26.25 mm (625 voxels)
Final image height	Up to 13 mm (800 to 1300 voxels)	Up to 98.2 mm (2340 voxels)
Voltage, current	70 kV, 114 µA	100 kV, 300 µA
Frame rate, Averaged frames	2 frames s^{-1}, 4	12 frames s^{-1}, 4
Number of projections per turn	1440	704
Stack mode	No	Yes
Imager mode	Full resolution (1920×1536 pixels)	Binning 2x2 (960×768 pixels)

Two configurations were used to scan the samples: a high-resolution (HR) scanning method and a fast low-resolution scanning (LR) method. LR scanning was performed on all the collected samples over their entire height. Owing to the HR scan duration of about 50 min for 1.3 cm of snow height (see below), HR scanning was not used systematically. When applied, HR scans were done on the same snow samples used for the LR scans, but only at specific heights of the samples. Figure 5 presents LR and HR scans co-located on the same snow sample. The tomography acquisition parameters used for the scans are detailed in Table 2 and briefly described below.

HR scans were obtained at a voxel size of 10 µm, a resolution that allows for capturing snow microstructure and directly deriving snow properties from the images. At this resolution, the field of view (the scanned snow volume) was 18.07×18.07 mm^2 in cross-section and 13.19 mm in height. Images were cropped during the reconstruction step to eliminate unusable image borders, so the size of the final cropped images was 12.5×12.5 mm^2 in cross-section and 8 to 13 mm in height. One HR scan lasted around 50 minutes. Note that HR scanning of samples of very light and fresh snow (with a high SSA) was sometimes not possible, as compaction occurred during the scan and led to an image of bad quality.

LR scanning was performed to capture the entire height of the collected snow sample in a time-efficient way, using a larger voxel size of 42 µm. A binning of 2×2 pixels was used: the effective resolution of the detector was artificially degraded, such that a 2×2 matrix of pixels was taken and combined to create one larger pixel. With that setup, the field of view was 37.92×37.92 mm^2 in cross-section. For the vertical dimension, we used the stack mode so that multiple LR scans were performed, each at different fixed vertical positions, and combined. This way, the entire height of the snow sample was imaged. The size of the final cropped images was 26.25×26.25 mm^2 in cross-section and up to 98.2 mm in height. With that, scanning was done at a speed of approximately 5 mm of snow height per minute.

2.3.3 Image analysis and property computation

The first step of the analysis was image registration. The LR scans were manually positioned in the snowpack height coordinates using the heights recorded during snow sampling in the field. The positions of the HR scans were then obtained by applying a

https://doi.org/10.5194/essd-2026-718
Preprint. Discussion started: 21 September 2026

registration operation that matched the HR scan (grayscale attenuation image) to the LR scan. The registration was performed using the package SimpleITK, by maximizing the correlation between the images using a linear gradient descent method. Results were visually checked for each scan.

Both the HR and LR scans were then segmented into a binary ice–air image using the energy-based method of Hagenmuller et al. (2013), in which the data term is derived from a fit of the attenuation histogram with the partial volume mixture model (Gage et al., 1992). The regularization parameter, which controls the level of smoothing, was adjusted separately for the HR and LR scans by visually optimizing the segmentation on images of various snow types and kept identical within each scan type.

Vertical profiles of snow properties were computed from the segmented images based on chord length distributions. For each horizontal slice of the LR and HR images, the distributions of ice and air chord lengths were computed in the vertical (z) and horizontal (x, y) directions, discarding chords intersecting the image borders. In addition, the 20 uppermost and lowermost slices of each sample were excluded to avoid border effects. The ice volume fraction, ϕ, was computed as the ratio of the cumulative ice chord length to the cumulative total (ice and air) chord length, both measured in the horizontal directions. Snow density was then obtained as $\rho = \phi\,\rho_{\mathrm{ice}}$, with ρ_{ice} = 917.5 kg m^{-3}. The SSA was derived from the mean ice chord length $\bar{L}$ averaged over the three directions using the stereological relationship $\mathrm{SSA} = 4/(\rho_{\mathrm{ice}}\bar{L})$. The structural anisotropy was defined as the ratio of the mean ice chord length in the vertical direction to that in the horizontal directions, $\mathcal{A} = 2\bar{L}_z/(\bar{L}_x + \bar{L}_y)$, where values below 1 indicate a preferentially horizontal structure, whereas values above 1 indicate a preferentially vertical structure. Microstructural properties derived from tomography images are primarily sensitive to image resolution and the applied image-processing method, with an impact that depends on the snow type considered (Flin et al., 2011; Hagenmuller et al., 2016). For SSA, comparisons with methane-adsorption measurements, considered as a reference, showed agreement within 3 % for tomography measurements acquired at a resolution of 30 μm (Kerbrat et al., 2008). For density, comparisons with gravimetric measurements showed agreement within 5 - 9 % (Proksch et al., 2016).

Because of their coarser resolution, the LR scans miss the thinnest chords and smooth out the finest structures, leading to biased estimates of SSA in particular. To mitigate this resolution effect, the chord length distributions of the LR scans were corrected before computing the snow properties. The number of chords of length L was multiplied by the transfer function

$$T(L) = \frac{1 + \exp\left[-(L/2\sigma_{\mathrm{LR}})^2\right]}{1 + \exp\left[-(L/2\sigma_{\mathrm{HR}})^2\right]}, \quad (1)$$

which enhances the contribution of short chords in the LR scans relative to the HR scans, where σ_{HR} and σ_{LR} characterize the effective smoothing of the HR and LR scans, respectively. These two parameters were calibrated using all pairs of co-located HR and LR scans: the chord length distributions of both scan types were accumulated over common 1-mm-thick layers, and σ_{HR} and σ_{LR} were optimized by minimizing the mean absolute differences in ice volume fraction and SSA between the corrected LR scans and the HR scans. The calibration yielded $\sigma_{\mathrm{HR}} = 4.1$ µm and $\sigma_{\mathrm{LR}} = 57.0$ µm, which can be interpreted as the effective resolutions of the two scan types, of the same order as their voxel sizes of 10 and 42 µm. Note that the same

https://doi.org/10.5194/essd-2026-718
Preprint. Discussion started: 21 September 2026

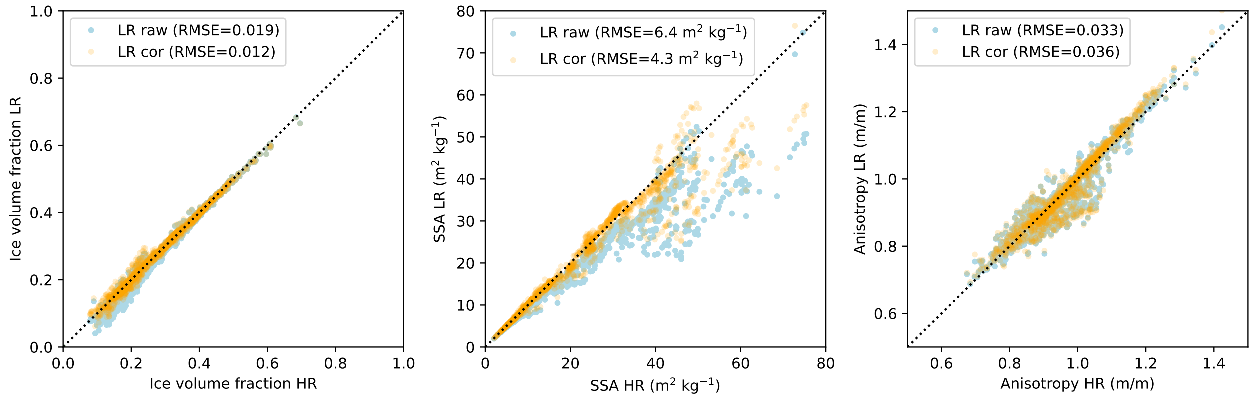

Figure 6. Correlation between ice volume fraction, SSA, and structural anisotropy estimated from the HR scans and the LR scans. Values from the LR scans before correction (LR raw, in blue) and after correction (LR cor, in orange) are provided.

HR–LR pairs were used for calibration and evaluation. However, because only two parameters were fitted using hundreds of layers, overfitting is unlikely. The performance of this correction is evaluated in Sec. 2.3.4.

Finally, vertical profiles of snow type were determined visually from the tomography images. The same operator (P. Hagenmuller) inspected each scan individually, divided it vertically into intervals of homogeneous snow type, and assigned to each interval a primary and, when relevant, a secondary snow type, following the morphological classification of the International Classification for Seasonal Snow on the Ground (Fierz et al., 2009). This classification was performed independently of the traditional snow profiles of the snowpack. Relying on a single operator ensured consistency of the classification across the whole dataset.

2.3.4 LR scan evaluation

Properties derived from the LR scans, before and after correction, are compared with those derived from the HR scans in Figure 6. Only overlapping HR and LR scans were used for the comparison. After correction, good agreement is obtained for the ice volume fraction (RMSE of 0.012): the slight underestimation observed in the raw LR data, mainly in recent snow where image resolution is most critical, disapears. For SSA and structural anisotropy, the scatter remains larger after correction; however, the RMSEs remain small, 4.3 $m^2\ kg^{-1}$ and 0.036, respectively. Nevertheless, LR scans tend to underestimate SSA, even after correction, for SSA values above 40 $m^2\ kg^{-1}$.

2.4 Cutter measurements

Two types of box-type density cutters were used to measure snow density, one of 100 cm^3 (3 cm height, 5.5 cm length, and 6 cm width) (e.g. Proksch et al., 2016), and one of 250 cm^3 (10 cm$\times$10 cm$\times$2.5 cm). A measurement error of about 10 % can be expected (Carroll, 1977; Conger and McClung, 2009; Proksch et al., 2016).

https://doi.org/10.5194/essd-2026-718
Preprint. Discussion started: 21 September 2026

During this campaign, cutter measurements were performed from the surface to the bottom of the snowpack, mostly with a regular vertical resolution of 3 cm. Regular sampling was not possible in some cases, for example, because of the presence of hard layers, so the vertical resolution of the measurements can vary.

2.5 DUFISSS measurements

The DUal Frequency Integrating Sphere for Snow SSA measurement (DUFISSS) is an optical system that measures the infrared hemispherical reflectance of snow, from which the snow SSA is derived (Gallet et al., 2009). For this, snow samples are collected in a sample holder of 6.3 cm diameter and 2.5 cm height, making sure to have a flat and even snow surface. When needed, the excess of snow is cut or gently pressed down. The snow samples are then placed in DUFISSS and illuminated using the 1310 nm light diode. The recorded voltage signals are then converted into reflectance values based on the voltage-to-reflectance calibration curve, obtained using the reflectance standard values. SSA values are finally derived from the reflectance values using the following polynomial fit, $\mathrm{SSA} = a_5 R_s^5 + a_4 R_s^4 + a_3 R_s^3 + a_2 R_s^2 + a_1 R_s + a_0$, with R_s the reflectance and $a_5 = 6526.67$, $a_4 = -10409.84$, $a_3 = 6878.49$, $a_2 = -2076.35$, $a_1 = 338.04$, $a_0 = -15.75$. This fit differs from the one presented in Gallet et al. (2009) (equation 9 in the paper). At the 1310 nm wavelength, measurement uncertainty is estimated below about 10 % for SSA values lower than 60 $\mathrm{m^2\ kg^{-1}}$ and 15 % for higher ones (Gallet et al., 2009).

During this campaign, DUFISSS measurements were performed from top to bottom along the snow pit wall, with a regular vertical resolution of 3 cm, when possible, except for the 11th, 18th, and 24th of January 2022, for which the resolution was 1 cm. Here again, the vertical resolution of the measurements varied in some cases, due to sampling difficulties. The instrument was thermalized outside before starting the measurement. The measurement of the reflectance standards was done at the beginning of the measurement procedure.

2.6 HISSGraS measurements

The Handheld Integrating Sphere Snow Grain Sizer (HISSGraS) is a field instrument recently developed by Aoki et al. (2023) to measure snow SSA. HISSGraS is based on the same measurement principle as DUFISSS (Gallet et al., 2009) and measures snow reflectance at 1310 nm. This instrument allows SSA measurements directly on a clean, smooth snow pit wall, so without having to sample snow. For that, the instrument is held facing the pit wall, and the measurement window, from which the light radiations come in and out, is gently pressed into the snow surface. The voltage-to-reflectance calibration curve is obtained based on the measured reflectance standard values. Reflectance values are converted into SSA using a theoretical reflectance-SSA relationship derived from a radiative transfer model based on Mie theory, assuming spherical snow grains (Aoki et al., 1999). The instrument can be equipped with a sheltering disk to prevent sunlight from penetrating into the instrument through the snow surface and disturbing the measurement.

HISSGraS measurements were carried out during the winter 2022–2023, following the direct measurement method. Profiles were measured from the top to the bottom of the snowpack with a regular vertical resolution of 3 cm, except for 31 January 2023, for which a resolution of 1 cm was used. We also measured SSA at the surface of the snowpack, placing the instrument vertically on the surface and using the sheltering disk.

https://doi.org/10.5194/essd-2026-718
Preprint. Discussion started: 21 September 2026

2.7 SMP measurements

The SnowMicroPen (SMP) is a motorized cone penetrometer measuring the vertical penetration resistance profile of the snowpack at high resolution (Johnson and Schneebeli, 1999; Schneebeli et al., 1999). The SMP is driven vertically into the snowpack at a constant speed of 20 mm s^{-1} to measure the penetration resistance exerted at the tip of the probe on a cone (diameter of 5 mm and cone half angle of 30°) with a vertical resolution of 1/242 mm.

Here, we used an SMP version 4 and measured with the SMP placed on a low table with adjustable feet. The threshold for the overload was set to 40 N. The measurements were done following the standard procedure, except in the case of early overloads, which occurred on February 22, March 1, and March 8, 2022. At these dates, the SMP reached the overload value before reaching the ground due to layers of hard snow. To allow for more complete SMP profiles, the SMP measurements that stopped before the ground due to an overload were repeated in the same hole, but after breaking the hard layers using an avalanche probe inserted in the SMP hole. We discarded the first 10 cm of the snow signal of the second SMP measurement, as the snow below the broken hard layers may have been disturbed. The data from the two SMP measurements of the same hole were then combined.

SMP data were quality checked and processed using the snowmicropyn package (URL: https://snowmicropyn.readthedocs.io/en/latest/). The air–snow and snow–ground interfaces were detected manually to remove the parts of the signal that correspond to air or ground. Density and SSA profiles were derived from the penetration force profiles, based on Proksch et al. (2015). First, the stochastic model of (Löwe and van Herwijnen, 2012) was applied to estimate the median of the penetration resistance force $\tilde{F}$ and a characteristic length of the microstructure L on a vertical window of size 1 mm with an overlap of 50%. A median operator was then applied to the 5 profiles of $\tilde{F}$ and L of each day to obtain a median profile. This operation smoothes the SMP data and mainly preserves variations that appear consistently in the 5 profiles. Finally, we applied the regressions of Calonne et al. (2020) to derive density and SSA from the median profile of $\tilde{F}$ and L, as

$$\rho_{\mathrm{smp}} = a_1 + a_2 \ln(\tilde{F}) + a_3 \ln(\tilde{F})\, L + a_4\, L \qquad \mathrm{SSA}_{\mathrm{smp}} = b_1 + b_2 \ln(L) + b_3 \ln(\tilde{F}) \tag{2}$$

with $a_1 = 295.8$, $a_2 = 65.1$, $a_3 = -43.2$, $a_4 = 47.1$, $b_1 = 0.57$, $b_2 = -18.56$, and $b_3 = -3.66$, and where ρ_{smp} is in kg m^{-3}, L in mm, $\tilde{F}$ in N, and $\mathrm{SSA}_{\mathrm{smp}}$ in m^2 kg^{-1}. The vertical resolution of the obtained density and SSA profiles is 0.5 mm.

3 Results

3.1 Seasonal evolution of the snowpack and atmospheric conditions

3.1.1 Winter 2021–2022

Figure 7 shows the temporal evolution of the atmospheric and snowpack conditions during the winter of 2021–2022. Figure 8 complements it by presenting the temporal evolution of the density profiles from the cutter measurements, SSA profiles from DUFISSS, and force profiles from the SMP. Climatological data from the previous 28 winters at Col de Porte are also provided for comparison: daily minimum, maximum, and quantile values of the hourly air temperature and hourly snow height from the

https://doi.org/10.5194/essd-2026-718
Preprint. Discussion started: 21 September 2026

Open Access Earth System Science Data Discussions

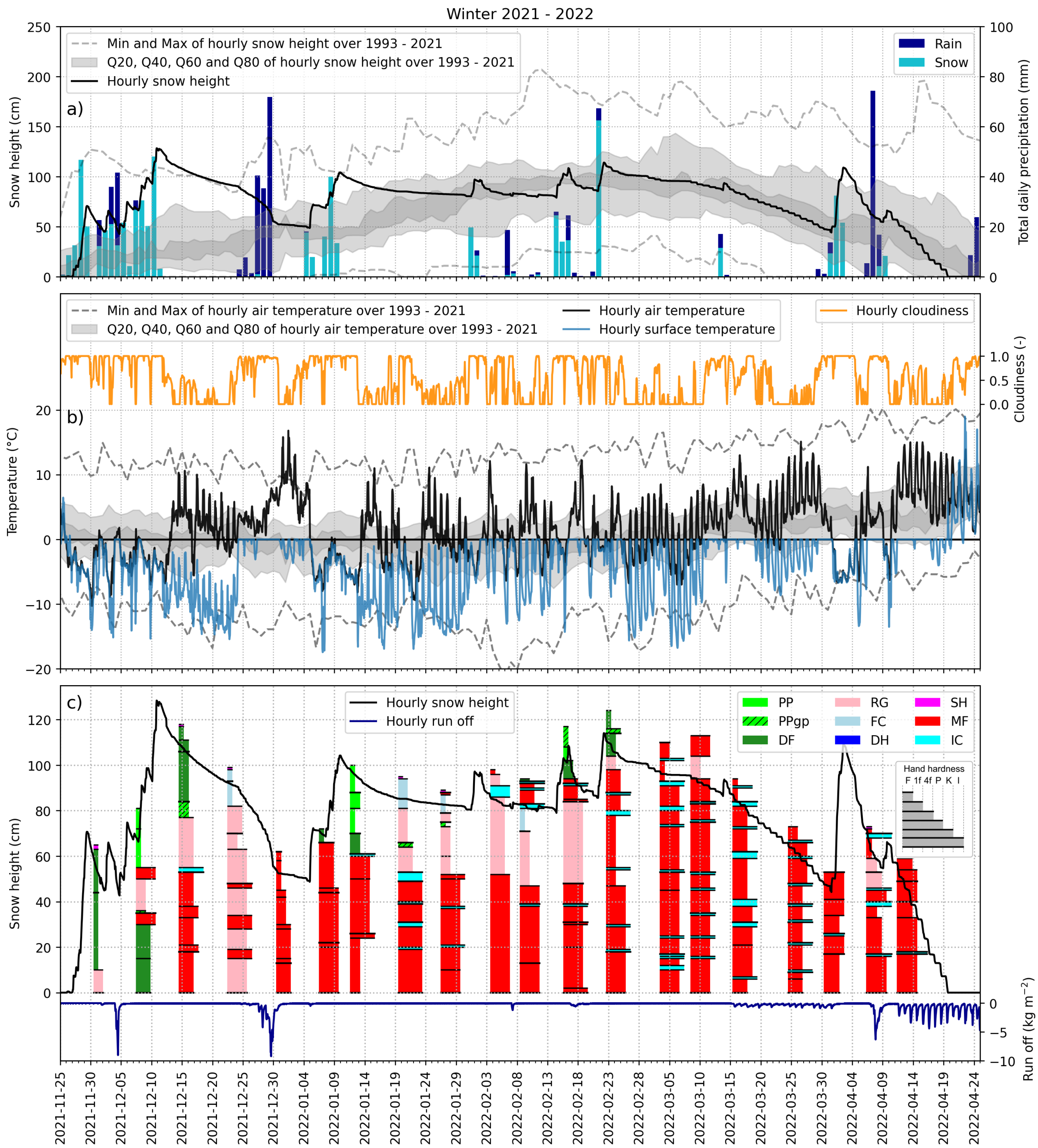

Figure 7. a) Hourly snow height and total daily precipitation from automatic measurements during winter 2021–2022. The minimum, the maximum, the 20th percentile (Q20), the 40th percentile (Q40), and the 60th percentile (Q60) of the hourly snow height data over the period 1993–2021 are provided for comparison. b) Hourly air temperature, hourly surface temperature, and hourly cloudiness from automatic measurements during winter 2021–2022. The minimum, the maximum, and the quantiles of the hourly air temperature data over the period 1993–2021 are provided. c) Snow profiles from the manual snow profiles, hourly snow height and basal water runoff from automatic measurements during winter 2021–2022. For each snow layer, the color indicates the primary snow type, and the width indicates the hand hardness, following Fierz et al. (2009).

https://doi.org/10.5194/essd-2026-718
Preprint. Discussion started: 21 September 2026

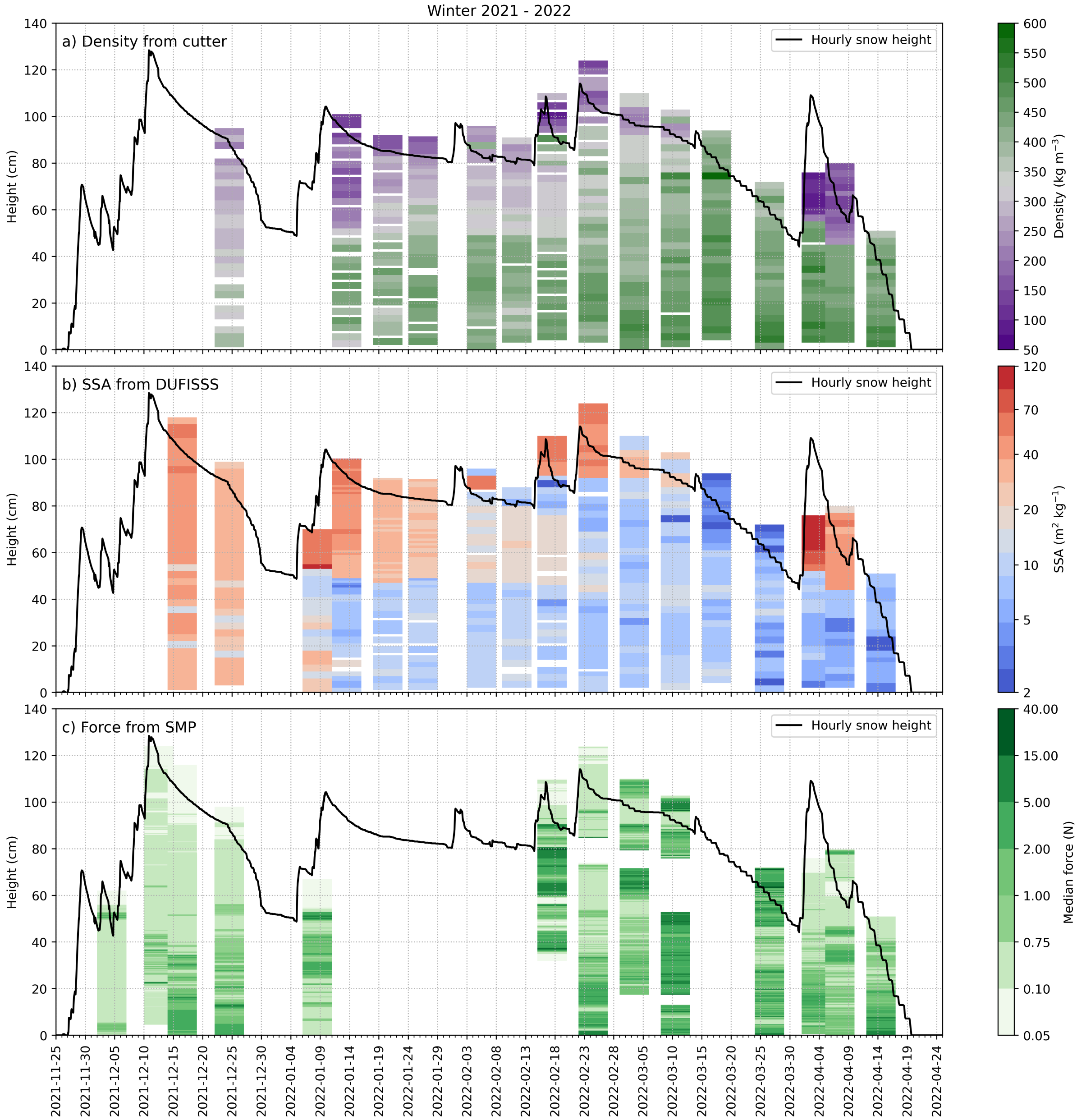

Figure 8. Temporal evolution of vertical snowpack properties during winter 2021 -2022. a) Density from the cutter measurements, b) SSA profiles from the DUFISSS measurements, and c) median penetration resistance force from the SMP measurements. Each vertical bar corresponds to one profile; the left side of the bar shows the measurement time. For visualization, the width of each bar is artificially set to correspond to 5 days. Hourly snow height from the automatic measurements is shown with black lines.

https://doi.org/10.5194/essd-2026-718
Preprint. Discussion started: 21 September 2026

winters of 1993–1994 to 2020–2021 are shown (Fig. 7), with a winter defined as the period from November 1 to April 30 of each year. Note that snow heights from the snow profiles and hourly snow heights from the automatic measurements can differ slightly because they are measured at locations 20 to 30 m apart; a mean deviation of 13 cm and an RMSD of 13 cm were estimated between the two locations by Lejeune et al. (2019).

The winter of 2021–2022 had continuous snow cover from November 26, 2021, to April 14, 2022. It was characterized by snow heights close to the climatological average, with a mean hourly snow height from November 1, 2021, to April 30, 2022, of 63 ± 37 cm, compared with 53 ± 44 cm over the 1993–2021 reference period. This corresponds to a snow-height anomaly of $+9.9$ cm (standardized anomaly: 0.2). The mean hourly air temperature was 1.9 ± 4.8°C, close to the reference value of 1.15 ± 5.2,°C over the 1993–2021 reference period, indicating no significant temperature anomaly. However, the total winter precipitation was 1092 kg m^{-2}, higher than the reference value of 989 kg m^{-2}.

We sum up the main weather events (Fig. 7.a and .b) and their consequences on the snowpack stratigraphy (Fig. 7.c) and snowpack properties (Fig. 8) in a chronological order.

- The winter started with a first period of regular snow precipitations, which brought the snowpack to a height of 128 cm on December 10, becoming the maximum snow height recorded on that day since 1993. Rainfall and snow surface temperatures of up to 0°C also occurred during that period. It led to a snowpack made of precipitation particles, decomposed and fragmented particles, and rounded grains, interrupted by melt forms, mostly melt-freeze crusts and ice crusts.

- Then, a dry weather period occurred from December 10 to 24, associated with rather low snow surface temperature, ranging from -5°C to -15°C over 15 days. This favored the formation of faceted crystals in the top first 20 cm, whereas the rest of the snowpack developed towards rounded grains, except for the crusts that remained (see the snow profile of December 22 in Fig 7.c). The snowpack settled down to about 90 cm.

- Between December 24 and 29, heavy rainfall occurred, with a total of around 150 mm of water. Consequently, the entire snowpack was affected by liquid water percolation and developed into melt forms. Snow height decreased rapidly to reach 50 cm. After the rain, warm air and snow surface temperatures continued until the beginning of January, keeping the snowpack wet (as indicated in the January 6 profile). This lower part, approximately 50 cm high, made of melt forms, persisted for the remainder of the season. The effect of the heavy rainfall is visible in the cutter and DUFISSS data (Fig. 8). A net transition in density and SSA is found around 50 cm height from the end of December 2021 on, that persisted until mid-February 2022. Below this height, the snow was dense, with densities mostly comprised between 400 and 500 kg m^{-3}, and had low SSA, mostly below 10 m^2 kg^{-1}, typical of melt forms.

- Conditions in January and February were normal, with the succession of snowfalls, dry periods, and small rainfalls. First, significant snowfalls occurred between January 4 and 9 and the snowpack reached a height of about 100 cm. These snowfalls were deposited on the wet snowpack formed during the heavy rain events. They formed layers that contrasted with the lower part of the snowpack, showing densities below 250 kg m^{-3} and SSA above 30 m^2 kg^{-1}. The rest of January was dry, and the recent snow developed into faceted crystals at the top and rounded grains below. February was

https://doi.org/10.5194/essd-2026-718
Preprint. Discussion started: 21 September 2026

Open Access Earth System Science Data Discussions

wetter and the snow surface temperature occasionally reached 0°C, mostly due to rain events, forming melt-freeze crusts and ice layers.

– Finally, from the beginning of March on, typical spring conditions prevailed, with snow surface melting during daytime. The snowpack gradually decreased in height, losing about 50 cm in a month. The snowpack consisted of melt forms interrupted by ice layers. About 60 cm of fresh snow fell on April 1, quickly melting and transforming into melt forms, to complete snow disappearance on April 20.

3.1.2 Winter season 2022–2023

The atmospheric and snowpack conditions during the winter of 2022–2023 are presented in Figs. 9 and 10. In contrast to the previous winter, snow cover remained sparse throughout most of the season. The longest period of continuous snow cover lasted only about 1.5 months, from January 9, 2023, to February 24, 2023. This was the earliest date of snowpack disappearance recorded at Col de Porte over the 1993–2021 reference period. The winter of 2022–2023 had by far the lowest snow cover among the 30 winters from 1993–1994 to 2022–2023. The mean hourly snow height from November 1, 2022, to April 30, 2023, was 7 ± 11 cm, compared with 53 ± 44 cm over the period 1993–2021. This corresponds to a snow-height anomaly of -46 cm (standardized anomaly: -1.04). The second-lowest winter, 2006–2007, had a mean snow height of 17 cm, more than twice that of 2022–2023. The mean hourly air temperature was $2.0 \pm 5.1\,°$C, close to the average value of $1.15 \pm 5.2\,°$C over the period 1993–2021, indicating no significant temperature anomaly. Total winter precipitation was 966 kg m^{-2}, slightly lower than the average value of 989 kg m^{-2} over the same period.

The temporal evolution of the atmospheric and snowpack properties was characterized by the following main events.

– A first thin snowpack formed end of November 2022, reached 22 cm height by mid-December, and completely melted by the end of December. The melt was caused by about 165 mm of rain over 72h from December 20 on. No snow property profiles were taken during this period.

– From December 25, 2022, to January 9, 2023, no snow was on the ground and the period was characterized by relatively warm air temperature, between about 5 to 10°C, and occasional rainfalls.

– From January 9, 2023, regular consecutive snowfalls started, characterized by a high proportion of graupels, and interspersed with rainy spells. By mid-January, the snowpack reached its maximum height of the entire season of 53 cm. As shown by the snow profile of January 20, the snowpack consisted of melt forms, topped by a thin ice layer, topped by mostly decomposed and fragmented particles (Fig 9.c). The entire snowpack had a low hardness, mostly 'fist' or '4 fingers', except for the ice layer. Consistently, this ice layer showed a high penetration force resistance, which stands out from the other layers and can be easily tracked over time, located at heights between 7 to 10 cm (Fig 10.c).

– A long dry period followed for almost 2 months, from January 19 to March 7, except for a few insignificant snowfalls that brought less than 5 cm of fresh snow. For the first 10 days of this period, from January 19 to February 1, relatively cold temperatures prevailed. Snow surface temperatures were never warmer than -5°C, and punctually as low as -15°C

https://doi.org/10.5194/essd-2026-718
Preprint. Discussion started: 21 September 2026

Earth System Science Data
Open Access Discussions

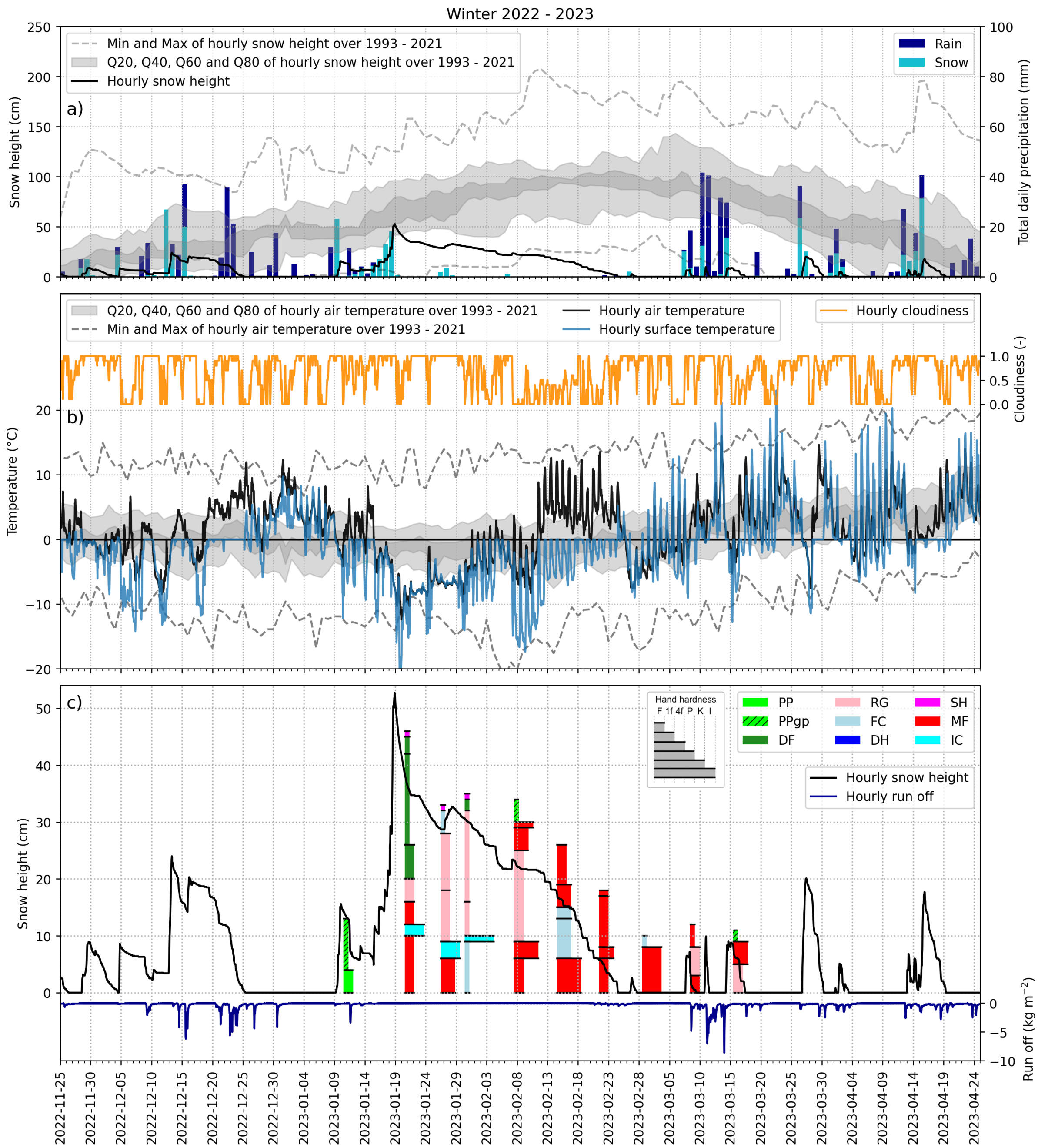

Figure 9. a) Hourly snow height and total daily precipitation during winter 2022–2023. The minimum, the maximum, the 20 quantile (Q20), the 40 quantile (Q40), and the 60 quantile (Q60) of the hourly snow height data over the period 1993–2021 are provided for comparison. b) Hourly air temperature, hourly surface temperature, and hourly cloudiness during winter 2022–2023. The minimum, the maximum, and the quantiles of the hourly air temperature data over the period 1993–2021 are provided. c) Snow profiles from the manual snow pits, hourly snow height, and hourly basal water runoff during winter 2022–2023. For each snow layer, the color indicates the primary snow type, and the width indicates the hand hardness, following Fierz et al. (2009).

https://doi.org/10.5194/essd-2026-718
Preprint. Discussion started: 21 September 2026

Open Access Earth System Science Data Discussions

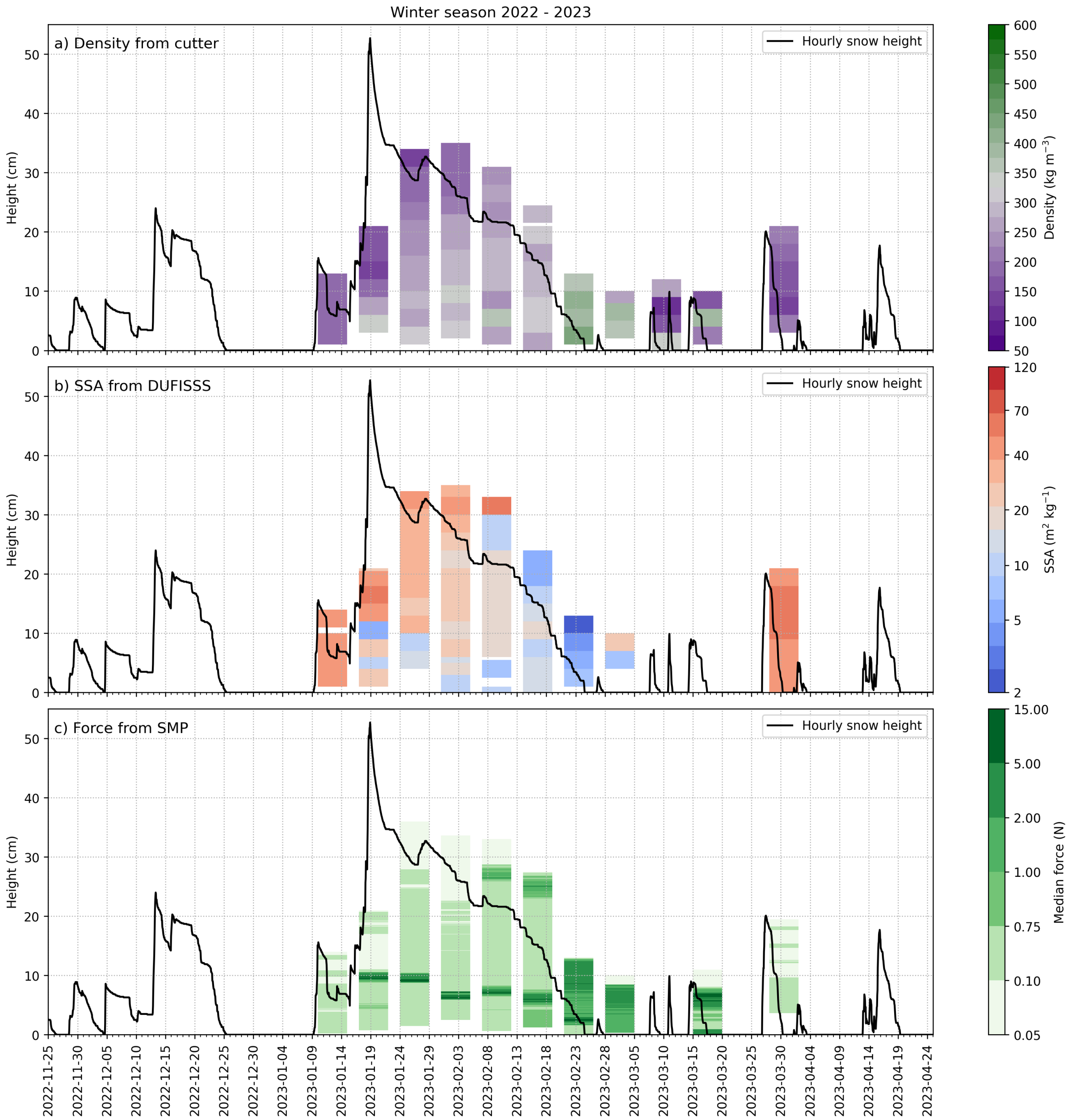

Figure 10. Temporal evolution of vertical snowpack properties during winter 2022–2023. a) Density from the cutter measurements, b) SSA profiles from the DUFISSS measurements, and c) median penetration resistance force from the SMP measurements. Each vertical bar corresponds to one profile; the left side of the bar shows the measurement time. For the sake of visualization, the width of each bar is artificially set to correspond to a duration of 5 days. Hourly snow height from the automatic measurements is shown with black lines.

https://doi.org/10.5194/essd-2026-718
Preprint. Discussion started: 21 September 2026

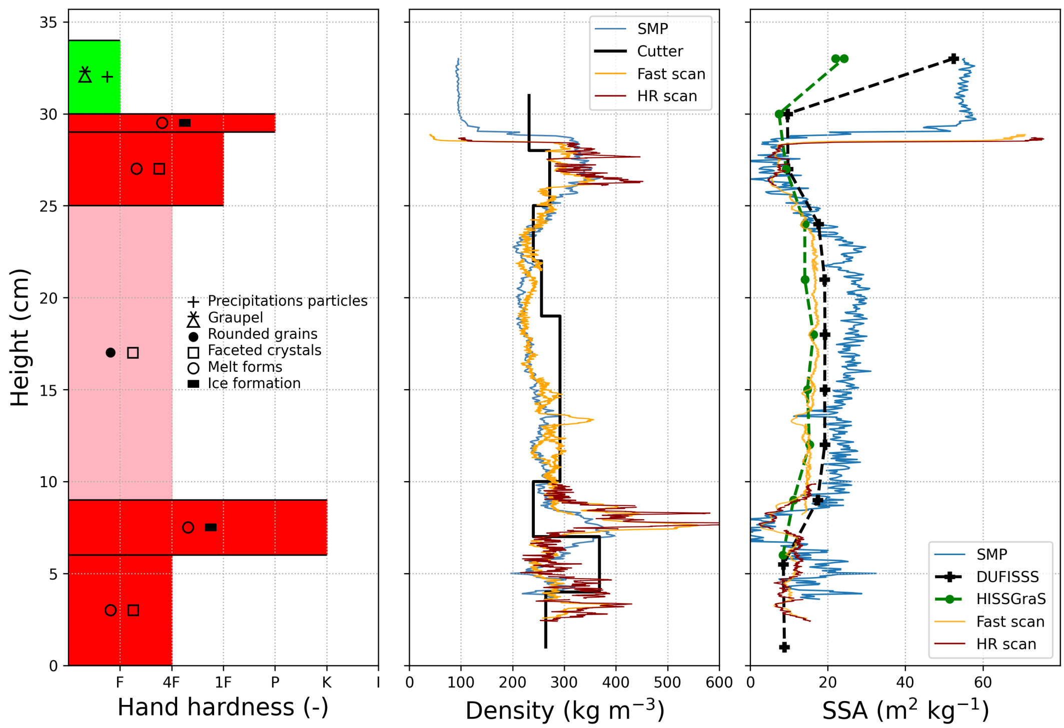

Figure 11. Snowpack stratigraphy from snow profiles and vertical profiles of density and SSA from the different measurement methods on February 7, 2023. The snowpack was dry.

to -20°C. It favored the formation and persistence of surface hoar and faceted crystals in the upper part of the snowpack. The ice layer formed with the rain of early January persisted at around 10 cm height, as shown by the snow profiles. The snowpack settled down to about 28 cm height by February 1. The rest of the dry period, from February 1 to March 7, was characterized by warmer temperatures. The diurnal cycle of the air temperature could be observed, and the snow surface reached 0°C almost daily during daytime, while the snow refroze at night. Air temperatures were consistently high, between 2 to 10°C, from mid-February on. As melt water percolates into the snowpack, melt forms gradually formed, associated with a decrease of SSA and an increase of density (see property profiles of February, 21 in Fig. 10). On February 22, the snowpack was fully made of melt forms and had strongly decreased in height (Fig 9.c). The snowpack fully melted by February 24 at the weather station location.

– The long dry period finally came to an end with the rainfall on March 7. Spring was rather wet, showing a mix of regular rain and snowfall. Several thin snowpacks formed with a height of 10 to 20 cm maximum, which lasted at most for a few days before complete melt.

https://doi.org/10.5194/essd-2026-718
Preprint. Discussion started: 21 September 2026

Open Access Earth System Science Data Discussions

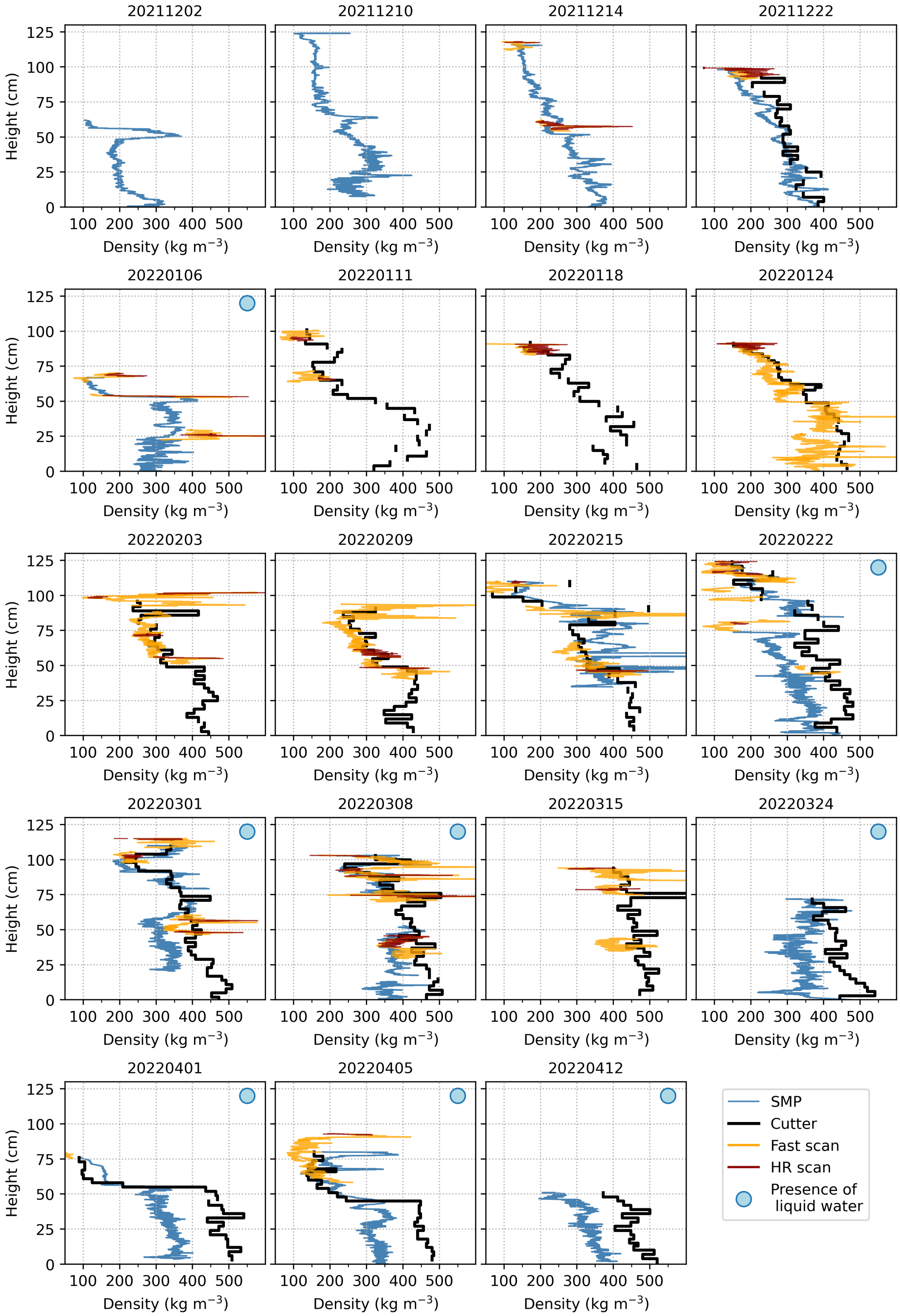

Figure 12. Density profiles obtained during winter 2021–2022 from the density cutter, SMP, LR scans, and HR scans. The presence of liquid water in the snowpack (partial or full) at the time of measurement is indicated by the blue symbol. When needed, a shift was applied to the heights of the SMP profiles to better match the cutter profiles (described in Sec. 3.2).

https://doi.org/10.5194/essd-2026-718
Preprint. Discussion started: 21 September 2026

Open Access Earth System Science Data Discussions

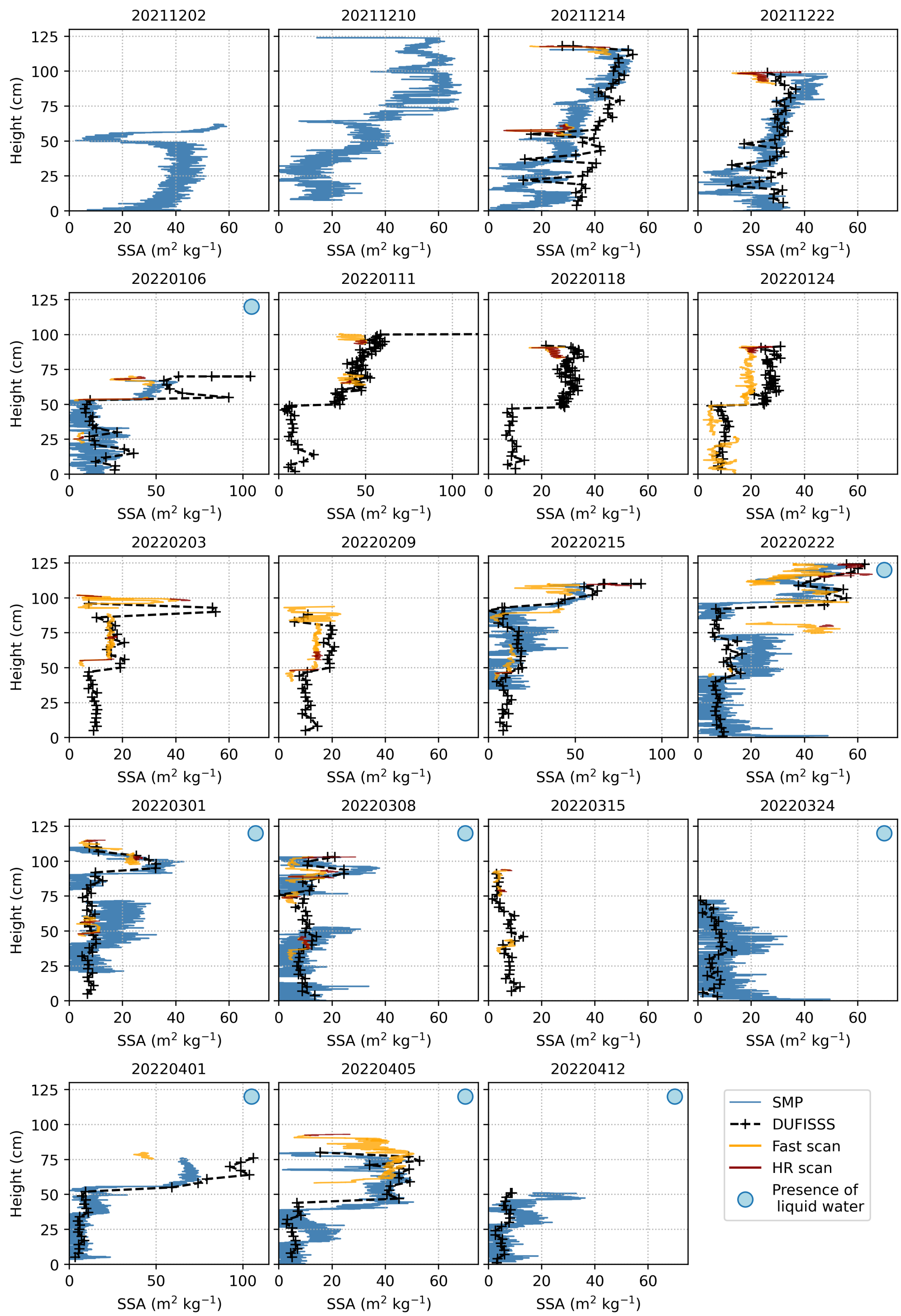

Figure 13. SSA profiles obtained during winter 2021–2022 from DUFISSS, SMP, LR scans, and HR scans. The presence of liquid water in the snowpack (partial or full) at the time of measurement is indicated by the blue symbol. When needed, a shift was applied to the heights of the SMP profiles to better match the DUFISSS profiles (described in Sec. 3.2).

https://doi.org/10.5194/essd-2026-718
Preprint. Discussion started: 21 September 2026

Open Access Earth System Science Data Discussions

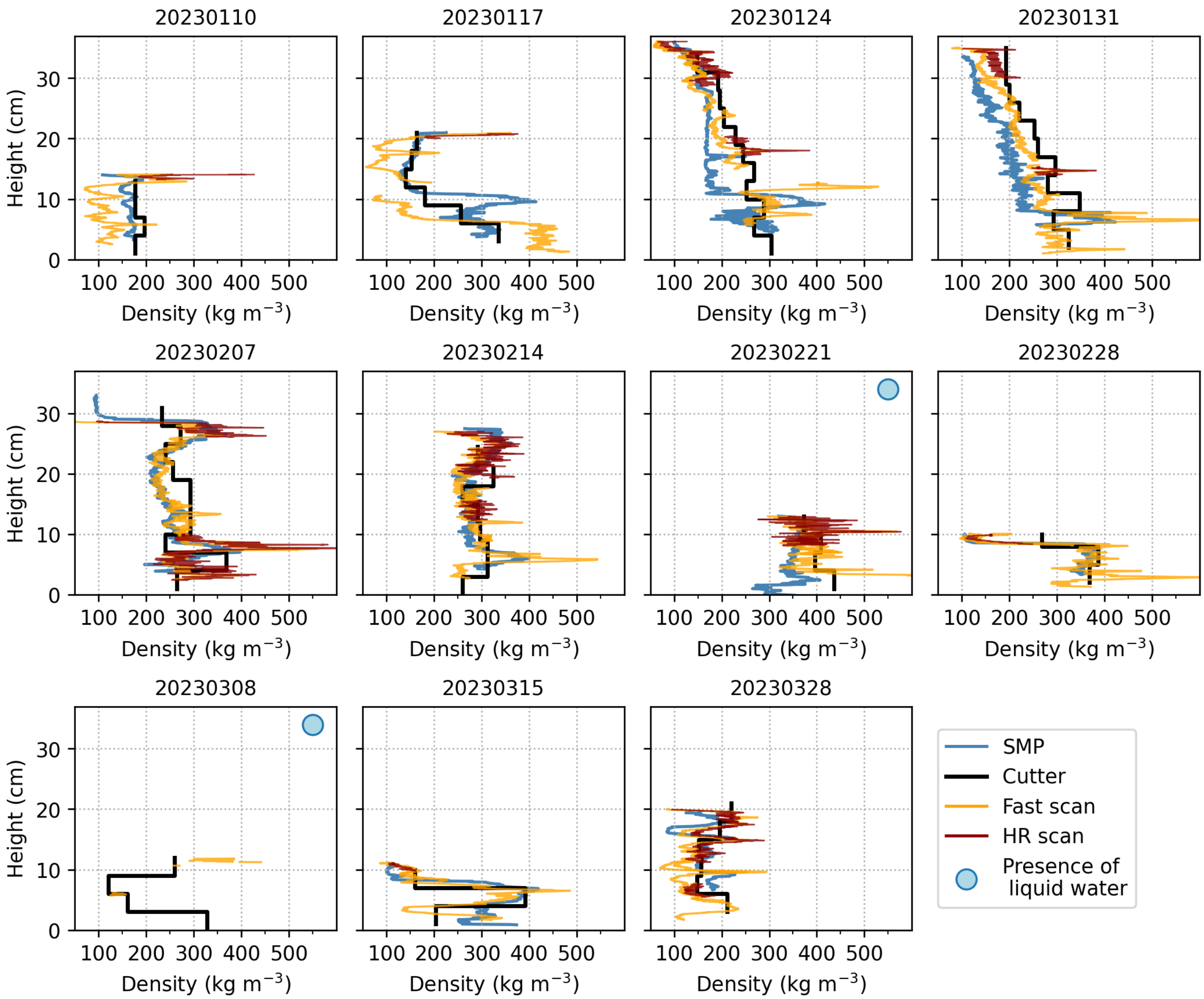

Figure 14. Density profiles obtained during winter 2022–2023 from the density cutter box, SMP, LR scans, and HR scans. The presence of liquid water in the snowpack (partial or full) at the time of measurement is indicated by the blue circle. When needed, a shift was applied to the heights of the SMP profiles to better match the cutter profiles (described in Sec. 3.2).

https://doi.org/10.5194/essd-2026-718
Preprint. Discussion started: 21 September 2026

Open Access Earth System Science Data Discussions

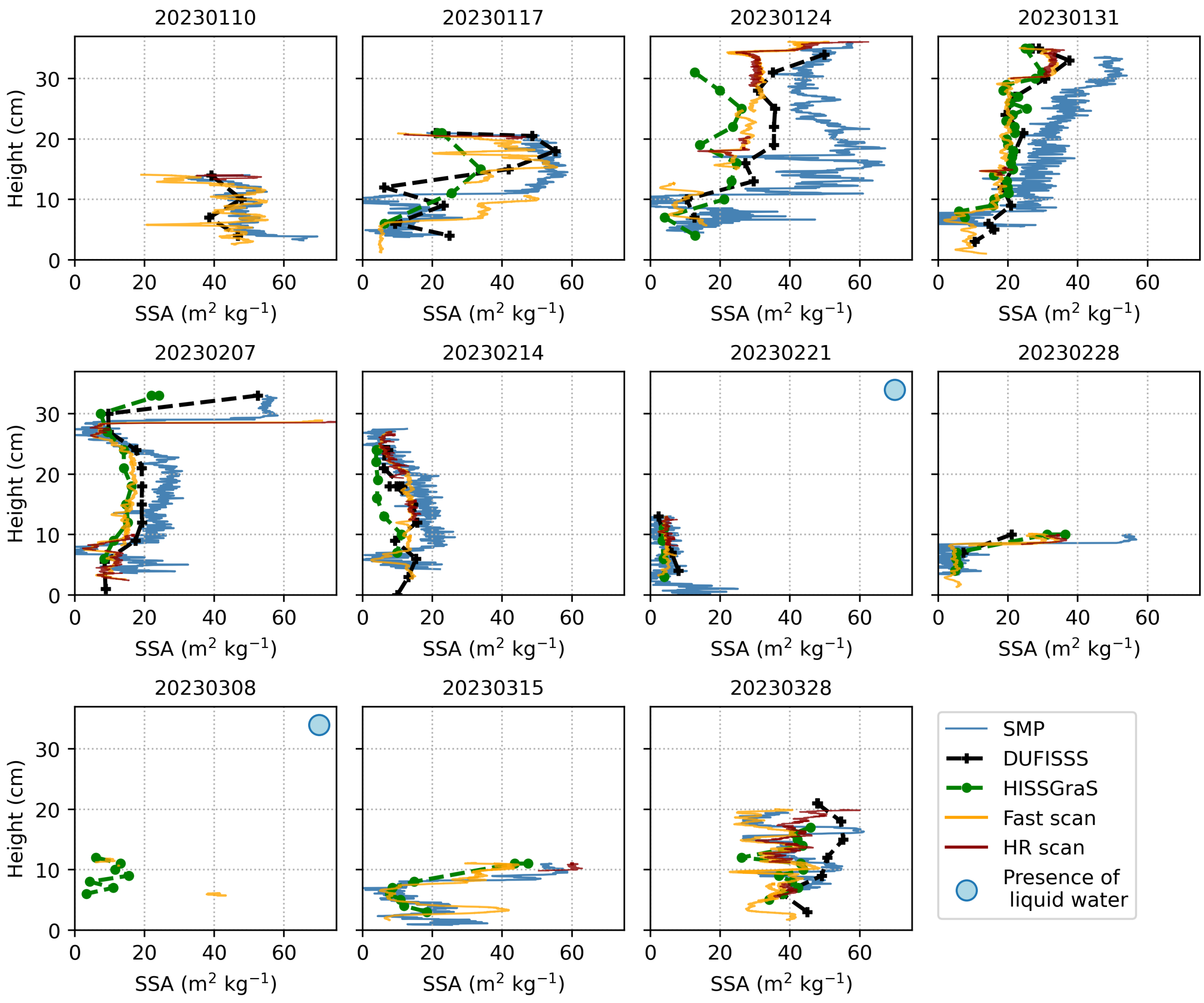

Figure 15. SSA profiles obtained during winter 2022–2023 from DUFISSS, SMP, HISSGraS, LR scans, and HR scans. The presence of liquid water in the snowpack (partial or full) at the time of measurement is indicated by the blue circle. When needed, a shift was applied to the heights of the SMP profiles to better match the DUFISSS profiles (described in Sec. 3.2).

https://doi.org/10.5194/essd-2026-718
Preprint. Discussion started: 21 September 2026

3.2 Vertical profiles of density and SSA from multiple instruments

We present the vertical profiles of snow density and SSA obtained during the two winter seasons from the SMP, density cutter, DUFISSS, HISSGraS, fast tomography (LR), and high-resolution tomography (HR) measurements. Figure 11 illustrates the dataset for February 7, 2023, together with the corresponding snow profile. The SMP and tomography measurements, owing to their higher vertical resolution, resolve finer density and SSA variations than the other methods.

Figure 12 to Figure 15 present an overview of the dataset and show the vertical profiles of density and SSA obtained from each instrument for each measurement day. To plot these profiles, a simple manual height realignment was applied to the SMP data to visually align prominent stratigraphic transitions with the cutter or DUFISSS profiles. It was only used when an obvious mismatch was found. 4 out of 13 SMP profiles were realigned for winter 2021–2022, and 6 out of 11 for winter 2022–2023. The applied vertical shift never exceeded 30% of the total snowpack height. The blue circle in the upper right corner of the plots indicates the presence of liquid water in the snowpack at the time of measurements, based on observer comments or, when available, co-temporal temperature profiles.

Overall, the density and SSA profiles are qualitatively consistent among the different measurement techniques, showing similar profile structures. A quantitative comparison between instruments cannot be performed without further profile processing. Indeed, as the measurements were collected at different locations along the snow pit wall, up to 1 m apart, spatial variability in the snowpack often results in vertical misalignment between profiles, as visible in Figs. 12 - 15. A direct comparison of the profiles would therefore be biased by spatial variability (Proksch et al., 2015). The provided profiles would require profile matching to enable a relevant quantitative instrument intercomparison (Hagenmuller and Pilloix, 2016). Such an analysis is beyond the scope of this paper. Nevertheless, noticeable discrepancies in the density and SSA derived from the SMP are observed for some measurement days and are discussed in Sec. 4.2. In addition, a dedicated quantitative comparison between the DUFISSS and HISSGraS instruments is presented in Sec. 4.1.

3.3 Snow-type characteristics from tomography

We analyze the relationships between snow type, density, SSA, and structural anisotropy over both winter seasons using properties derived from tomography measurements. The distributions of these properties by snow type are shown in Fig. 16. To emphasize the characteristic properties of each snow type, only samples with identical primary and secondary snow types were retained. The mixed FC/DH class was included as an exception because no pure DH samples were observed. Results for all primary-secondary snow-type combinations are presented in Appendix Fig. A1.

Over both winters, the most represented snow types are by far MF and the mixed type RG/FC (Fig. A1). No pure DH was observed, as is typical for Col de Porte (Lejeune et al., 2019). The PP class often consisted of rimed PP and graupel (PPgp), which is also typical of Col de Porte.

The density and SSA distributions reproduce the expected differences among snow types (e.g., Colbeck, 1991; Fierz et al., 2009; Domine et al., 2007). From Figure 16 showing the values for non-mixed snow types, PP, DF, and SH exhibit the lowest densities, with median values between 150 and 170 kg m^{-3}. Recent snow (PP and DF) has the highest SSA values (around 40

https://doi.org/10.5194/essd-2026-718
Preprint. Discussion started: 21 September 2026

Open Access Earth System Science Data Discussions

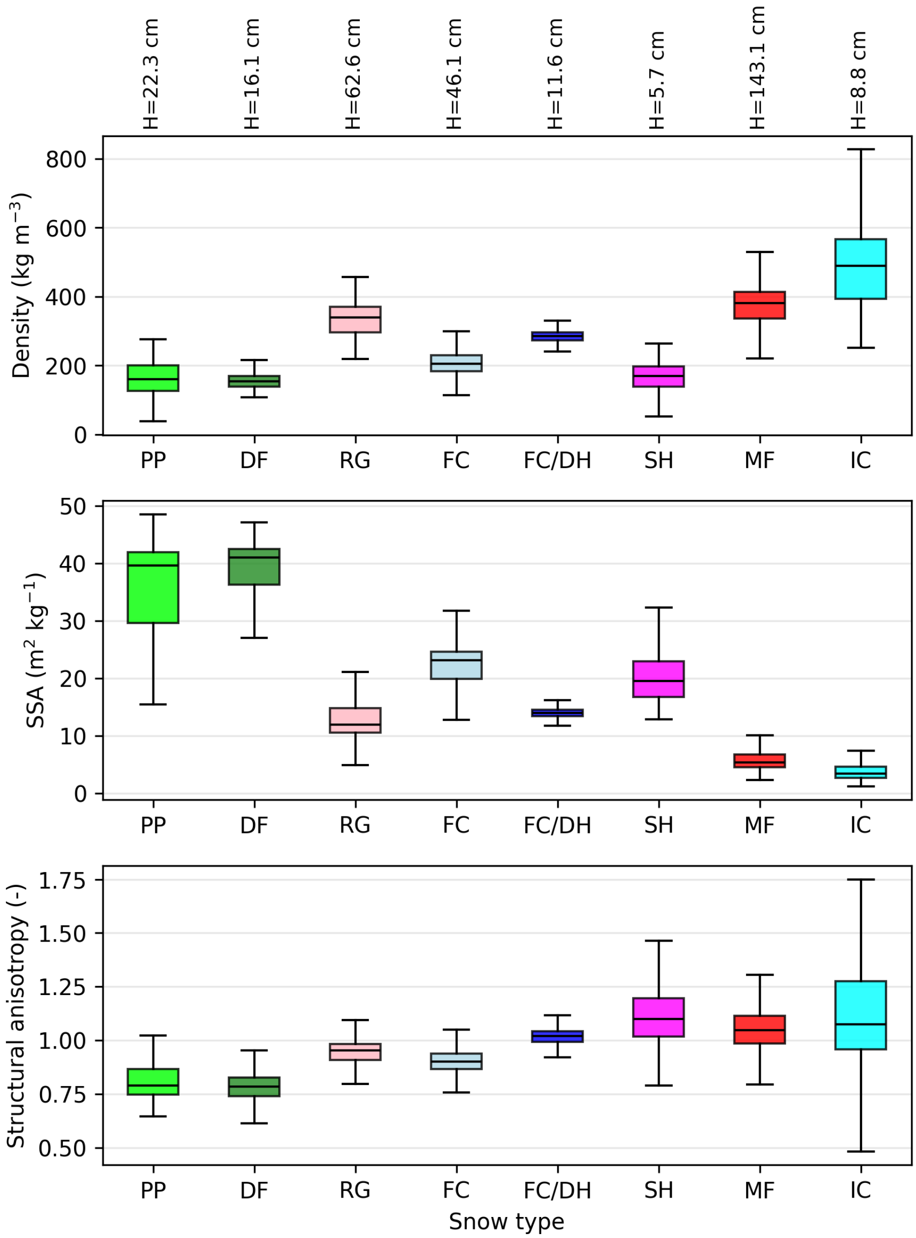

Figure 16. Distribution of density, SSA, and structural anisotropy derived from tomography measurements, grouped by snow type identified from the 3D images. Boxes extend from the 25th to the 75th percentiles, horizontal lines indicate the medians, and whiskers indicate the minimum and maximum values. H is the cumulative height of the analyzed layers. Only snow layers with identical primary and secondary snow types are included, except for the mixed FC/DH class, which is retained because no pure DH layers were observed. The abbreviations of the snow type names follow the international classification for seasonal snow on the ground (Fierz et al., 2009).

https://doi.org/10.5194/essd-2026-718
Preprint. Discussion started: 21 September 2026

$m^2\ kg^{-1}$), whereas SH displays intermediate SSA values comparable to those of FC (around 20 $m^2\ kg^{-1}$). In contrast, MF and IC have the highest densities, up to a median of 480 kg m^{-3}, and lowest SSA values, down to 3 to 5 $m^2\ kg^{-1}$, while RG and FC occupy intermediate ranges.

Regarding structural anisotropy, PP and DF exhibit a pronounced preferential horizontal structure, with median structural anisotropy values of 0.78. This horizontal orientation nearly vanishes in RG, whose median approaches 0.95, but remains more pronounced in FC, with a median of 0.90, reflecting that the anisotropy inherited from freshly fallen snow seems better preserved in FC than in RG. This observation is consistent with the density and SSA values of the FC, which remain closer to those of fresh snow than RG (median density of 205 versus 340 kg m^{-3}, and median SSA of 23 versus 12 $m^2\ kg^{-1}$). The stronger compaction experienced by RG may contribute to the greater loss of the initial anisotropy. The FC/DH class does not display the pronounced vertical anisotropy commonly associated with well-developed depth hoar, for which values as high as 1.35 have been reported (e.g. Bouvet et al., 2023). The MF snow type is also nearly isotropic, with a median value of 1.04, suggesting that wet-snow metamorphism does not generate a marked preferential orientation. Rather, it tends to remove the horizontal anisotropy inherited from recent snow: for example, the mixed MF/PP class has a median anisotropy of 0.94, compared with 0.78 for pure PP (Appendix Fig. A1). SH exhibits a preferential vertical orientation, although with substantial variability. Finally, IC also has a median anisotropy slightly above 1, but its very broad distribution indicates highly variable structures.

4 Discussion

4.1 Comparing SSA from the DUFISSS and HISSGraS instruments

During the winter of 2022–2023, SSA measurements obtained with the recently developed HISSGraS instrument can be compared with those from the other methods, particularly DUFISSS, which is based on the same measurement principle. The SSA profiles are generally consistent, but HISSGraS systematically reports slightly lower SSA values than DUFISSS (Fig. 15). This difference is illustrated by the profiles from February 7, 2023 (Fig. 11).

To investigate this bias, measurements with both instruments were performed on the same snow samples on January 24 and January 31, 2023. Snow samples were collected following the DUFISSS sampling protocol using the dedicated sample holder and were subsequently measured with both DUFISSS and HISSGraS. Thus, unlike the standard HISSGraS measurements conducted during the campaign, these measurements were not performed directly along the pit wall. Using the same snow samples eliminates the influence of snowpack spatial variability. The comparison is presented in Fig. 17. On the two evaluated dates, HISSGraS reports lower SSA values than DUFISSS, with a mean bias (HISSGraS−DUFISSS) of $-3.69\ m^2\ kg^{-1}$ and an RMSE of $4.55\ m^2\ kg^{-1}$. The discrepancy is smaller for low SSA values.

Aoki et al. (2023) compared HISSGraS with IceCube, which relies on the same measurement principle as DUFISSS (Zuanon, 2013). Using 161 paired measurements performed on the same snow samples, they found good agreement overall between the two instruments, with noticeable discrepancies only for some high-SSA near-surface layers. They attributed these discrepancies either to snow evolution between successive measurements or to changes in the snow sample surface induced by contact with

https://doi.org/10.5194/essd-2026-718
Preprint. Discussion started: 21 September 2026

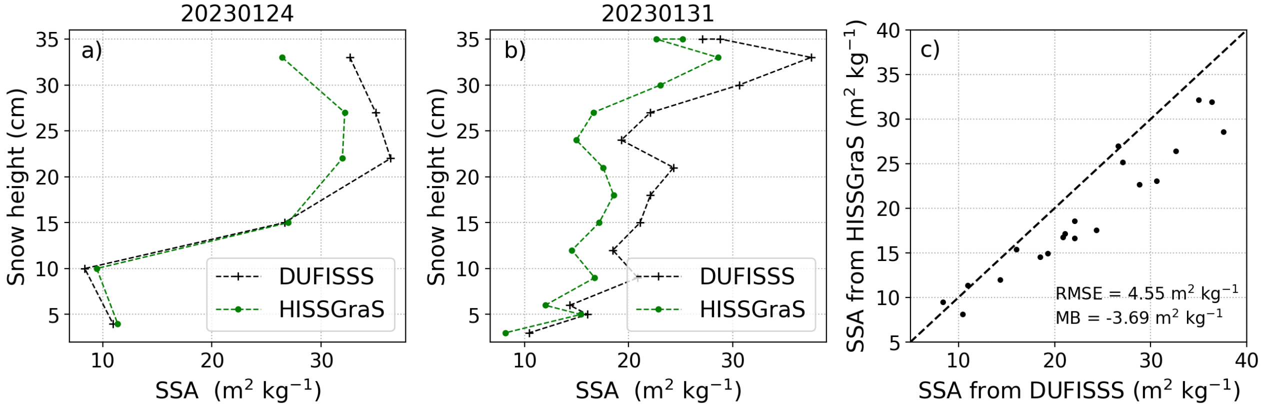

Figure 17. Comparison of SSA values between DUFISSS and HISSGraS using measurements performed on the same snow samples. a) and b) SSA profiles from January 24 and January 31, 2023, respectively. c) Correlation between SSA values measured with DUFISSS and HISSGraS, including the RMSE and mean bias (MB; HISSGraS−DUFISSS).

a relatively warm instrument window. In contrast, for the two dates investigated here, HISSGraS generally reports lower SSA values than DUFISSS at intermediate to high SSA values, with the discrepancy increasing with SSA. Given the limited scope of our comparison, Dedicated measurements under controlled laboratory conditions are needed to enable a more rigorous comparison of the two instruments.

4.2 Limitations of SMP measurements in warm snowpacks

Two main challenges were encountered during the SMP measurements. The first challenge is the penetration of hard snow layers, such as melt-freeze crusts and ice layers. When the probe encounters such layers, the maximum penetration force (overload) is reached and the measurement stops automatically to protect the force sensor. This leads to incomplete vertical force profiles. Because of the frequent alternation of melting and refreezing conditions at Col de Porte, hard layers occur frequently and often persist throughout the winter, resulting in incomplete SMP profiles over extended periods. During our campaign, at least one complete SMP profile was obtained on most measurement days from the five daily SMP measurements. On three days, however, all five measurements stopped before reaching the bottom of the snowpack because of an overload, typically near the middle of the snowpack. In these cases, an avalanche probe was used to break the hard layer responsible for the overload, and the SMP measurement was restarted in the same hole following the procedure described in Sec. 2.7. We therefore reconstructed complete force profiles by combining two successive SMP measurements, except across the hard layer itself. This was the case on February 22, 2022, as illustrated in Figure 18. The ice layers at 88 and 80 cm caused an overload. No SMP data are available for those heights. However, by applying the procedure mentioned above, we were able to get data in the part of the snowpack below. Density and SSA profiles from such reconstructed force profile can also be seen for March 1 and March 8, 2022 (Fig. 12 and 13).

https://doi.org/10.5194/essd-2026-718
Preprint. Discussion started: 21 September 2026

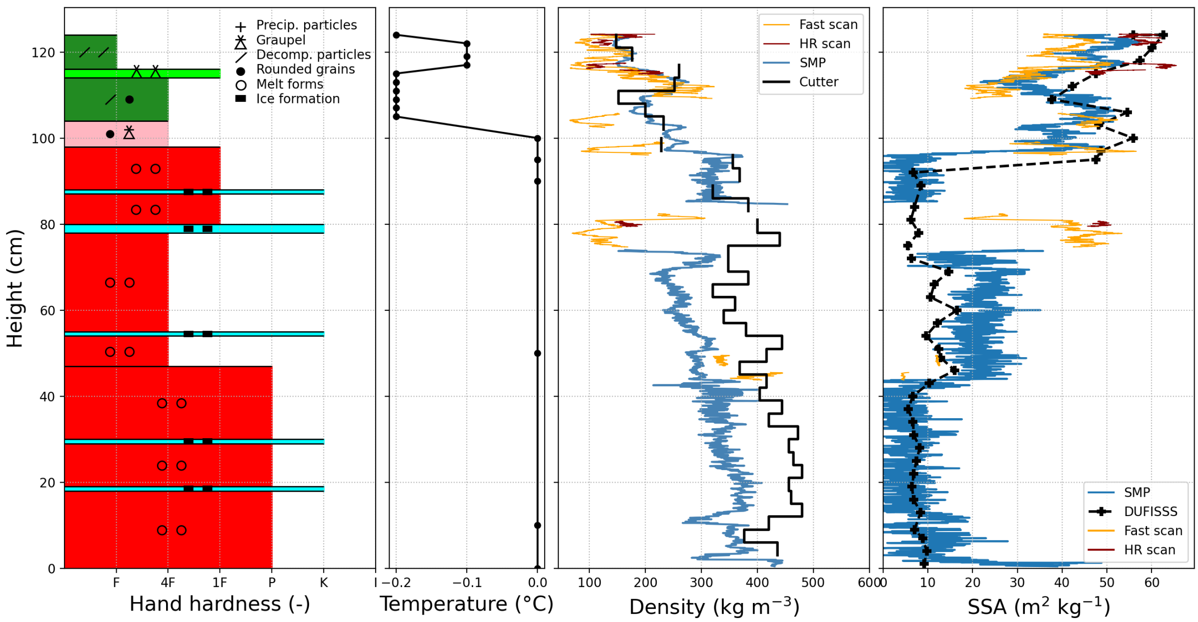

Figure 18. Snowpack stratigraphy and temperature from snow profiles, and vertical profiles of density and SSA from the different measurements for February 22, 2022. Note that the snow and temperature profiles were recorded at 2pm30, while the other measurements were performed between 10am30 and 12am30, local times.

The second challenge is that the empirical relationships used to derive snow density and SSA from SMP measurements are currently only valid for dry snow (Löwe and van Herwijnen, 2012; Proksch et al., 2015). At relatively warm sites such as Col de Porte, liquid water is frequently present in the snowpack, limiting the applicability of these relationships. The effect of wet snow on the derivation of density and SSA from the force signal can be seen in the vertical profiles in Figure 12 to 15, and in more detail for a particular day in Figure 18. The blue circle symbol in the vertical profiles indicates the presence of liquid water in the snowpack during the measurements. On February 22, 2022, the snowpack was dry in its upper part and wet in its lower part. As a consequence, density values from the SMP measurements agree well with the other data in the upper part of the snowpack, while below 80 cm height, they are systematically underestimated, by approximately 100 kg m^{-3}. Concerning the SSA values from the SMP measurements, no clear impact of the presence of liquid water could be detected. During the winter season 2021–2022, 8 measurement days showed a snowpack with liquid water in its bottom part. Similar observations can be made from these profiles: underestimated density values from the SMP are shown in the lower part of the profiles and seem to be associated with a transition from dry to wet snow (Fig. 12 to 15). The presence of liquid water during the SMP measurements is only approximate because it is inferred from observer's field observations, when available, or from temperature profiles acquired during snow profiling, which were not always recorded simultaneously with the SMP measurements. Dedicated measurements combining SMP and liquid water content observations would help quantify the influence of liquid water on the force signal. Developing methods to retrieve snow microstructural properties from SMP

https://doi.org/10.5194/essd-2026-718
Preprint. Discussion started: 21 September 2026

measurements in wet snow would extend the applicability of the technique to warm, low-altitude snowpacks such as Col de Porte and to spring melt conditions.

4.3 Snow layer tracking and profile matching

The tracking of specific snow layers over time was proposed as a way to compare snow properties obtained from different measurements or to evaluate snow models against observations through the temporal evolution of snow layer properties (Calonne et al., 2020). It requires snow layers whose boundaries can be distinguished from the surrounding layers and that persist for a sufficiently long period of time. Only a few layers could be tracked in our dataset. During winter 2021–2022, the marked transition in density and SSA located at a height of about 50 cm can be tracked in the cutter and DUFISSS data from the beginning of January to mid-February (Fig. 8). This transition separated the lower melt-forms layer from the upper part of the snowpack, which consisted mainly of rounded grains (Fig. 7.c). During winter 2022–2023, another trackable feature is a thin ice layer located at heights of 7–10 cm, which can be followed for about a month, from mid-January to mid-February (Fig. 10). It is particularly well identified in the SMP data by its high penetration-force resistance. This ice layer was formed in early January 2023 due to rain, as described in Sec. 3.1.2. These examples highlight the importance of the spatial and temporal resolution of the measurements for snow layer tracking. The higher vertical resolution of the SMP measurements provides a more detailed description of the snowpack stratigraphy than the cutter and DUFISSS measurements, which have a vertical sampling interval of 3 cm. For example, the ice layer described above is clearly visible in the SMP data but only weakly resolved in the cutter and DUFISSS data. Regarding temporal resolution, the weekly resolution of our measurements limits layer tracking, as it is difficult to follow the evolution of snow layers between successive measurements, except for sharp, contrasting snowpack transitions. As shown by Calonne et al. (2020), a daily temporal resolution is therefore more appropriate, as applied in current snowpack monitoring programs (e.g. Löwe et al., 2025).

Another method to compare snow properties from different sources is profile matching (Hagenmuller and Pilloix, 2016; Herla et al., 2021). This method aligns profiles based on corresponding stratigraphic features and can be used to compare profiles obtained with different measurement techniques or from simulations and observations. As described in Sec. 3.2, profile matching could be applied to the density and SSA profiles of our dataset to reduce vertical misalignment resulting from spatial variability. This could enable a quantitative instrument intercomparison based on our dataset, provided that satisfactory matching can be achieved. Profile matching can only compensate for discrepancies between profiles to a certain extent; measurements intended for comparison should therefore be performed as close to each other as possible to limit spatial variability, and with a consistent vertical reference to minimize initial offsets between profiles. These requirements were not specifically considered in our measurement protocol.

4.4 Tomography for snowpack monitoring

In this study, we assessed the feasibility of monitoring snowpack evolution by X-ray tomography over complete winter seasons. Because tomography requires rapid transport of snow samples to a cold laboratory, the infrastructure available at Col de Porte is particularly well suited to this approach. Obtaining undisturbed centimeter-scale snow samples proved to be the first practical

https://doi.org/10.5194/essd-2026-718
Preprint. Discussion started: 21 September 2026

challenge, especially for fragile fresh snow, which tended to compact during insertion into the sample holder, and for dense ice layers, which were difficult to cut through.

The second challenge concerns the trade-off between scan duration and image resolution. HR scanning is not practical for imaging complete alpine snowpacks, as scanning a 1-m snowpack would require approximately 80 hours under our current acquisition settings. We therefore complemented the HR scans with LR scans at a voxel size of 42 µm, which require only about 2 minutes per centimeter of snow height. HR scans were acquired on selected samples and used as reference data, whereas LR scans were applied more frequently to complete or large sections of the snowpack to retrieve continuous profiles of density, SSA, and structural anisotropy.

The LR scans were processed with the same segmentation and chord-length analysis as the HR scans, and thus provide the same set of properties – density, SSA, structural anisotropy – over the entire height of the samples, at a fraction of the acquisition time. Once the correction of the chord length distributions is calibrated on a limited set of co-located HR scans, LR scanning alone is sufficient to retrieve accurate property profiles: after correction, the agreement with the HR scans is within 0.012 in ice volume fraction, 4.3 m^2 kg^{-1} in SSA, and 0.036 in structural anisotropy (Sec. 2.3.4). This makes LR scanning a practical approach for the routine monitoring of snowpack microstructure. Its main limitations concern the finest microstructures, with SSA underestimated above about 40 m^2 kg^{-1}, and the computation of detailed microstructural descriptors, such as surface curvature, for which HR scans remain necessary. Emerging deep-learning-based super-resolution methods, which reconstruct fine microstructural details from low-resolution tomographic images, could further reduce these limitations and extend the applicability of fast scanning (e.g. Klos et al., 2025).

Overall, our study suggests that tomography is a promising tool for monitoring the microstructural evolution of natural snowpacks, provided that sufficient laboratory infrastructure and scanning time are available. It provides access to snow properties that cannot currently be measured with field instruments, such as structural anisotropy. The choice of image resolution and scan duration should be guided by the scientific objectives, the available resources, and the expected snow depth at the study site.

5 Conclusions

During the winters of 2021–2022 and 2022–2023, the IVORI field campaigns were carried out at Col de Porte as a complement to the standard observation program (Lejeune et al., 2019). The resulting dataset comprises two winter-long time series of vertical profiles of snow density, SSA, and structural anisotropy derived from complementary measurement techniques. In particular, X-ray tomography was applied to monitor snowpack evolution over complete winter seasons. This was made possible by the availability of an on-site cold laboratory equipped with a micro-CT scanner. Two tomography configurations were employed: fast scanning (LR) at a voxel size of 42 µm and high-resolution scanning (HR) at 10 µm. Measurements from the SnowMicroPen, density cutters, and two optical reflectance instruments (DUFISSS and HISSGraS) complement the tomography data, together with traditional snow profiles. Meteorological data from the Col de Porte automatic weather station are also provided to place the snowpack evolution in its atmospheric context.

The dataset provides a valuable benchmark for the evaluation of snow models under warm alpine conditions, where melt forms, including melt-freeze crusts, are frequent. The forcing dataset of atmospheric and soil properties at Col de Porte is available in Lejeune et al. (2019). The high vertical resolution of tomography and SMP measurements enables detailed characterization of snowpack stratigraphy. Despite the weekly sampling frequency, some persistent snow layers can still be tracked over time.

This study also highlights the complementary strengths and limitations of the different measurement techniques. Tomography provides access to microstructural information that is currently inaccessible to field instruments, but its application remains constrained by scan duration and the need to collect undisturbed snow samples. In contrast, the SMP allows for high-resolution snow property measurements in the field but remains limited in the presence of liquid water and hard snow layers. Future work should focus on extending SMP signal interpretation to wet snow and on improving the retrieval of microstructural properties from low-resolution tomography images, thereby expanding the applicability of both techniques to long-term snowpack monitoring.

Together, these observations constitute a comprehensive multi-instrument dataset that will support future studies of seasonal snowpack evolution, the evaluation and development of snow models, and the advancement of snow observation techniques.

6 Data availability

The dataset, including the field measurements and tomography data, is available at https://doi.org/10.6084/m9.figshare.33426472 (Calonne et al., 2026). The atmospheric and ground measurements and snow profiles from the Col de Porte observatory used in this study are available at https://doi.osug.fr/public/CRYOBSCLIM_CDP/CRYOBSCLIM.CDP.2018.html (Lejeune et al., 2019).

Author contributions. Neige Calonne wrote the manuscript with contributions from Lisa Bouvet, Marie Dumont, and Pascal Hagenmuller. Neige Calonne, Pascal Hagenmuller, Rémi Granger, Kévin Fourteau, Marie Dumont, Julien Brondex, François Tuzet, Yves Lejeune, Anne Dufour, and Mathieu Fructus performed the measurements. Teruo Aoki provided the HISSGraS instrument for the SSA measurements and contributed to the discussion of the SSA comparison. Rémi Granger and Pascal Hagenmuller processed and analyzed the tomography measurements. Neige Calonne and Lisa Bouvet processed and analyzed the field measurements. Marie Dumont conceived and coordinated the IVORI project.

Competing interests. The authors declare that they have no conflict of interest.

Acknowledgements. This research has been supported by the European Research Council (ERC) under the European Union's Horizon 2020 research and innovation program (IVORI; grant no. 949516). We thank Jacques Roulle for his support with the cold-laboratory and Victor

https://doi.org/10.5194/essd-2026-718
Preprint. Discussion started: 21 September 2026

Nussbaum, Axel Bouchet, Matthieu Lafaysse, and Alvaro Robledano for their help in the field measurements. We thank RX-Solutions for their support with the tomograph.

https://doi.org/10.5194/essd-2026-718
Preprint. Discussion started: 21 September 2026

Open Access Earth System Science Data Discussions

Appendix A

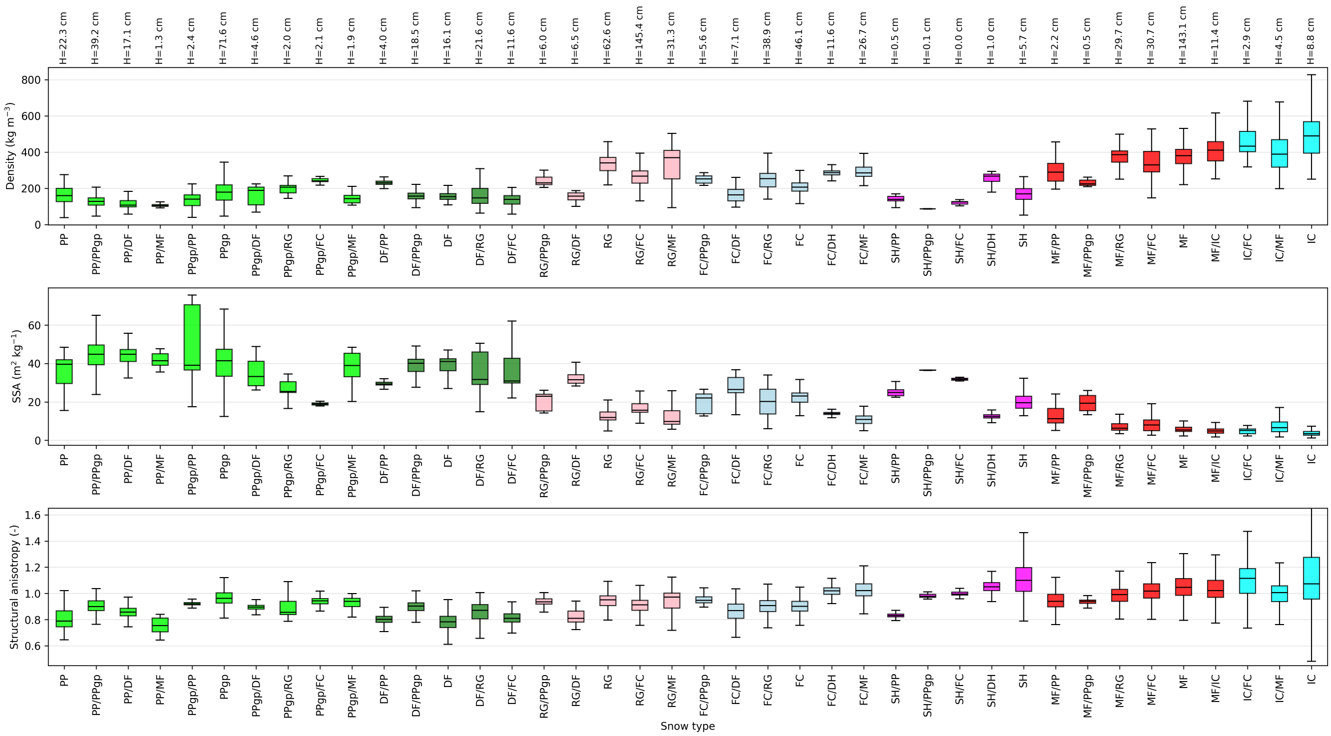

Figure A1. Distribution of density, SSA, and structural anisotropy derived from tomography measurements, grouped by snow type identified from the tomography images. Boxes extend from the 25th to the 75th percentiles, horizontal lines indicate the medians, and whiskers indicate the minimum and maximum values. H is the cumulative height of the analyzed samples.

https://doi.org/10.5194/essd-2026-718
Preprint. Discussion started: 21 September 2026

References

Aoki, T., Aoki, T., Fukabori, M., and Uchiyama, A.: Numerical simulation of the atmospheric effects on snow albedo with a multiple scattering radiative transfer model for the atmosphere-snow system, Journal of the Meteorological Society of Japan. Ser. II, 77, 595–614, https://doi.org/10.2151/jmsj1965.77.2_595, 1999.

Aoki, T., Hachikubo, A., Nishimura, M., Hori, M., Niwano, M., Tanikawa, T., Sugiura, K., Inoue, R., Yamaguchi, S., Matoba, S., et al.: Development of a handheld integrating sphere snow grain sizer (HISSGraS), Annals of Glaciology, pp. 1–12, https://doi.org/10.1017/aog.2023.72, 2023.

Bader, H.: Mineralogische und strukturelle Charakterisierung des Schnees und seiner Metamorphose, in: Der Schnee und seine Metamorphose, edited by Bader, H. et al., pp. 1–61, Kümmerly & Frey, Bern, https://books.google.com/books?id=-2V8RQAACAAJ, Beiträge zur Geologie der Schweiz, Geotechnische Serie Hydrologie 3, 1939.

Bouvet, L., Calonne, N., Flin, F., and Geindreau, C.: Heterogeneous grain growth and vertical mass transfer within a snow layer under a temperature gradient, The Cryosphere, 17, 3553–3566, https://doi.org/10.5194/tc-17-3553-2023, 2023.

Calonne, N., Richter, B., Löwe, H., Cetti, C., ter Schure, J., Van Herwijnen, A., Fierz, C., Jaggi, M., and Schneebeli, M.: The RHOSSA campaign: multi-resolution monitoring of the seasonal evolution of the structure and mechanical stability of an alpine snowpack, The Cryosphere, 14, 1829–1848, https://doi.org/10.5194/tc-14-1829-2020, 2020.

Calonne, N., Flin, F., Morin, S., Lesaffre, B., du Roscoat, S. R., and Geindreau, C.: Numerical and experimental investigations of the effective thermal conductivity of snow, Geophysical Research Letters, 38, L23 501, https://doi.org/10.1029/2011GL049234, 2011.

Calonne, N., Flin, F., Geindreau, C., Lesaffre, B., and Rolland du Roscoat, S.: Study of a temperature gradient metamorphism of snow from 3-D images: time evolution of microstructures, physical properties and their associated anisotropy, The Cryosphere, 8, 2255–2274, https://doi.org/10.5194/tc-8-2255-2014, 2014.

Calonne, N., Hagenmuller, P., Granger, R., Bouvet, L., Fourteau, K., Brondex, J., Tuzet, F., Lejeune, Y., Dufour, A., Fructus, M., Aoki, T., and Dumont, M.: Dataset of "Seasonal evolution of a warm alpine snowpack: a multi-instrument dataset of snow microstructure at Col de Porte, French Alps", https://doi.org/10.6084/m9.figshare.33426472, 2026.

Carroll, T.: A comparison of the CRREL 500 cm 3 tube and the ILTS 200 and 100 cm 3 box cutters used for determining snow densities, Journal of Glaciology, 18, 334–337, https://doi.org/10.3189/S0022143000021420, 1977.

Colbeck, S. C.: The layered character of snow covers, Reviews of Geophysics, 29, 81–96, https://doi.org/10.1029/90RG02351, 1991.

Coléou, C., Lesaffre, B., Brzoska, J.-B., Ludwig, W., and Boller, E.: Three-dimensional snow images by X-ray microtomography, Ann. Glaciol., 32, 75–81, https://doi.org/10.3189/172756401781819418, 2001.

Conger, S. M. and McClung, D. M.: Comparison of density cutters for snow profile observations, J. Glaciol, 55 (189), 163 – 169, https://doi.org/10.3189/002214309788609038, 2009.

Domine, F., Taillandier, A.-S., Houdier, S., Parrenin, F., Simpson, W. R., and Douglas, T. A.: Interactions between snow metamorphism and climate: Physical and chemical aspects, in: Physics and Chemistry of Ice, edited by Kuhs, W. F., pp. 27–46, Royal Society of Chemistry, Cambridge, UK, https://doi.org/10.1039/9781847557773, 2007.

Dumont, M., Monteiro, D., Filhol, S., Gascoin, S., Marty, C., Hagenmuller, P., Morin, S., Choler, P., and Thuiller, W.: The European Alps in a changing climate: physical trends and impacts, Comptes Rendus. Géoscience, 357, 25–42, https://doi.org/10.5802/crgeos.288, 2025.

Essery, R., Morin, S., Lejeune, Y., and Bauduin-Ménard, C.: A comparison of 1701 snow models using observations from an alpine site, Adv. Water Res., 55, 131–148, https://doi.org/10.1016/j.advwatres.2012.07.013, 2013.

https://doi.org/10.5194/essd-2026-718
Preprint. Discussion started: 21 September 2026

Essery, R., Kontu, A., Lemmetyinen, J., Dumont, M., and Ménard, C. B.: A 7-year dataset for driving and evaluating snow models at an Arctic site (Sodankylä, Finland), Geoscientific Instrumentation, Methods and Data Systems, 5, 219–227, https://doi.org/10.5194/gi-5-219-2016, 2016.

Fierz, C., Armstrong, R. L., Durand, Y., Etchevers, P., Greene, E., McClung, D. M., Nishimura, K., Satyawali, P. K., and Sokratov, S. A.: The international classification for seasonal snow on the ground, IHP-VII Technical Documents in Hydrology n 83, IACS Contribution n 1, https://unesdoc.unesco.org/ark:/48223/pf0000186462, 2009.

Flin, F., Lesaffre, B., Dufour, A., Gillibert, L., Hasan, A., Rolland du Roscoat, S., Cabanes, S., and Pugliese, P.: On the computations of specific surface area and specific grain contact area from snow 3-D images, in: Physics and Chemistry of Ice 2010, edited by Furukawa, Y., Sazaki, G., Uchida, T., and Watanabe, N., pp. 321–328, Hokkaido University Press, Sapporo, Japan, ISBN 978-4-8329-0361-6, https://www.hup.gr.jp/items/65002415, 2011.

Gage, H. D., Santago II, P., and Snyder, W. E.: Quantification of brain tissue through incorporation of partial volume effects, in: Medical Imaging VI: Image Processing, vol. 1652, pp. 84–96, SPIE, https://doi.org/10.1117/12.59414, 1992.

Gallet, J.-C., Domine, F., Zender, C. S., and Picard, G.: Measurement of the specific surface area of snow using infrared reflectance in an integrating sphere at 1310 and 1550 nm, The Cryosphere, 3, 167 – 182, https://doi.org/10.5194/tc-3-167-2009, 2009.

Hagenmuller, P.: TomoCold: Tomographie par rayons X en chambre froide, Réunion méthodes de caractérisation de la neige, https://www.osug.fr/missions/recherche/ateliers-transversaux/neige/evenement-scientifiques-passes/reunion-methodes-de-caracterisation-de-la-neige-08-03-2019.html, oSUG, Grenoble, France, 8 March 2019, 2019.

Hagenmuller, P. and Pilloix, T.: A new method for comparing and matching snow profiles, application for profiles measured by penetrometers, Frontiers in Earth Science, 4, 52, https://doi.org/10.3389/feart.2016.00052, 2016.

Hagenmuller, P., Chambon, G., Lesaffre, B., Flin, F., and Naaim, M.: Energy-based binary segmentation of snow microtomographic images, Journal of glaciology, 59, 859–873, https://doi.org/10.3189/2013JoG13J035, 2013.

Hagenmuller, P., Matzl, M., Chambon, G., and Schneebeli, M.: Sensitivity of snow density and specific surface area measured by microtomography to different image processing algorithms, The Cryosphere, 10, 1039–1054, https://doi.org/10.5194/tc-10-1039-2016, 2016.

Herla, F., Horton, S., Mair, P., and Haegeli, P.: Snow profile alignment and similarity assessment for aggregating, clustering, and evaluating snowpack model output for avalanche forecasting, Geoscientific Model Development, 14, 239–258, https://doi.org/10.5194/gmd-14-239-2021, 2021.

Hock, R., Rasul, G., Adler, C., Cáceres, B., Gruber, S., Hirabayashi, Y., Jackson, M., Kääb, A., Kang, S., Kutuzov, S., et al.: High mountain areas, in: IPCC special report on the ocean and cryosphere in a changing climate, pp. 131–202, H.-O. Pörtner, DC Roberts, V. Masson-Delmotte, P. Zhai, M. Tignor, E . . . , https://doi.org/10.1017/9781009157964.004, 2019.

Johnson, J. B. and Schneebeli, M.: Characterizing the microstructural and micromechanical properties of snow, Cold Regions Science and Technology, 30, 91–100, https://doi.org/10.1016/S0165-232X(99)00013-0, 1999.

Kerbrat, M., Pinzer, B., Huthwelker., T., Gäggeler, H. W., Ammann, M., and Schneebeli, M.: Measuring the specific surface area of snow with X-ray tomography and gas adsorption: comparison and implications for surface smoothness, Atmos. Chem. Phys., 8, 1261 – 1275, https://doi.org/10.5194/acp-8-1261-2008, 2008.

Klos, A., Salvo, L., and Lhuissier, P.: Super-resolution X-ray tomography using deep learning applied to the 3D quantification of defects in lattice structures, Scientific Reports, 15, 36 664, https://doi.org/10.1038/s41598-025-20372-4, 2025.

Krinner, G., Derksen, C., Essery, R., Flanner, M., Hagemann, S., Clark, M., Hall, A., Rott, H., Brutel-Vuilmet, C., Kim, H., Ménard, C. B., Mudryk, L., Thackeray, C., Wang, L., Arduini, G., Balsamo, G., Bartlett, P., Boike, J., Boone, A., Chéruy, F., Colin, J., Cuntz, M., Dai, Y., Decharme, B., Derry, J., Ducharne, A., Dutra, E., Fang, X., Fierz, C., Ghattas, J., Gusev, Y., Haverd, V., Kontu, A., Lafaysse, M., Law, R., Lawrence, D., Li, W., Marke, T., Marks, D., Ménégoz, M., Nasonova, O., Nitta, T., Niwano, M., Pomeroy, J., Raleigh, M. S., Schaedler, G., Semenov, V., Smirnova, T. G., Stacke, T., Strasser, U., Svenson, S., Turkov, D., Wang, T., Wever, N., Yuan, H., Zhou, W., and Zhu, D.: ESM-SnowMIP: assessing snow models and quantifying snow-related climate feedbacks, Geoscientific Model Development, 11, 5027–5049, https://doi.org/10.5194/gmd-11-5027-2018, 2018.

Krol, Q. and Löwe, H.: Relating optical and microwave grain metrics of snow: The relevance of grain shape, The Cryosphere, 10, 2847–2863, https://doi.org/10.5194/tc-10-2847-2016, 2016.

Lejeune, Y., Dumont, M., Panel, J.-M., Lafaysse, M., Lapalus, P., Le Gac, E., Lesaffre, B., and Morin, S.: 57 years (1960–2017) of snow and meteorological observations from a mid-altitude mountain site (Col de Porte, France, 1325 m of altitude), Earth System Science Data, 11, 71–88, https://doi.org/10.5194/essd-11-71-2019, 2019.

Lemmetyinen, J., Derksen, C., Rott, H., Macelloni, G., King, J., Schneebeli, M., Wiesmann, A., Leppänen, L., Kontu, A., and Pulliainen, J.: Retrieval of effective correlation length and snow water equivalent from radar and passive microwave measurements, Remote Sensing, 10, 170, https://doi.org/10.3390/rs10020170, 2018.

Löwe, H. and van Herwijnen, A.: A Poisson shot noise model for micro-penetration of snow, Cold Reg. Sci. Technol., 70, 62–70, https://doi.org/10.1016/j.coldregions.2011.09.001, 2012.

Löwe, H., Riche, F., and Schneebeli, M.: A general treatment of snow microstructure exemplified by an improved relation for thermal conductivity, The Cryosphere, 7, 1473–1480, https://doi.org/10.5194/tc-7-1473-2013, 2013.

Löwe, H., Proksch, M., Reuter, B., Calonne, N., Richter, B., Jaggi, M., Mewes, L., Schneebeli, M., Dadic, R., and Walter, B.: WFJ_DailySMP - High-Resolution Snow Stratigraphy at Weissfluhjoch – Davos 2015-ongoing, https://doi.org/10.16904/envidat.641, 2025.

Macfarlane, A. R., Schneebeli, M., Dadic, R., Tavri, A., Immerz, A., Polashenski, C., Krampe, D., Clemens-Sewall, D., Wagner, D. N., Perovich, D. K., et al.: A database of snow on sea ice in the central Arctic collected during the MOSAiC expedition, Scientific Data, 10, 398, https://doi.org/10.1038/s41597-023-02273-1, 2023.

Marty, C. and Meister, R.: Long-term snow and weather observations at Weissfluhjoch and its relation to other high-altitude observatories in the Alps, Theoretical and Applied Climatology, 110, 573–583, https://doi.org/10.1007/s00704-012-0584-3, 2012.

Ménard, C. B., Essery, R., Barr, A., Bartlett, P., Derry, J., Dumont, M., Fierz, C., Kim, H., Kontu, A., Lejeune, Y., Marks, D., Niwano, M., Raleigh, M., Wang, L., and Wever, N.: Meteorological and evaluation datasets for snow modelling at 10 reference sites: description of in situ and bias-corrected reanalysis data, Earth System Science Data, 11, 865–880, https://doi.org/10.5194/essd-11-865-2019, 2019.

Morin, S., Lejeune, Y., Lesaffre, B., Panel, J.-M., Poncet, D., David, P., and Sudul, M.: An 18-years long (1993 - 2011) snow and meteorological dataset from a mid-altitude mountain site (Col de Porte, France, 1325 m alt.) for driving and evaluating snowpack models, Earth Syst. Sci. Data, 4, 13–21, https://doi.org/10.5194/essd-4-13-2012, 2012.

Proksch, M., Löwe, H., and Schneebeli, M.: Density, specific surface area, and correlation length of snow measured by high-resolution penetrometry, Journal of Geophysical Research: Earth Surface, 120, 346–362, https://doi.org/10.1002/2014JF003266, 2015.

Proksch, M., Rutter, N., Fierz, C., and Schneebeli, M.: Intercomparison of snow density measurements: bias, precision, and vertical resolution, The Cryosphere, 10, 371–384, https://doi.org/10.5194/tc-10-371-2016, 2016.

Robledano, A., Picard, G., Dumont, M., Flin, F., Arnaud, L., and Libois, Q.: Unraveling the optical shape of snow, Nature Communications, 14, 3955, https://doi.org/10.1038/s41467-023-39671-3, 2023.

Schleef, S. and Loewe, H.: X-ray microtomography analysis of isothermal densification of new snow under external mechanical stress, J. Glaciol., 59, 214, https://doi.org/10.3189/2013JoG12J076, 2013.

https://doi.org/10.5194/essd-2026-718
Preprint. Discussion started: 21 September 2026

Schneebeli, M., Pielmeier, C., and Johnson, J. B.: Measuring snow microstructure and hardness using a high resolution penetrometer, Cold Reg. Sci. Technol., 30 (1–3), 101–114, https://doi.org/10.1016/S0165-232X(99)00030-0, 1999.

Védrine, L., Hagenmuller, P., Gélébart, L., Montagnat, M., and Bernard, A.: Role of ice mechanics on snow viscoplasticity, Geophysical Research Letters, 51, e2023GL107 676, https://doi.org/10.1029/2023GL107676, 2024.

Zuanon, N.: IceCube, a portable and reliable instruments for snow specific surface area measurement in the field, in: International Snow Science Workshop Grenoble-Chamonix Mont-Blance-2013 proceedings, pp. 1020–1023, https://arc.lib.montana.edu/snow-science/item/1905, 2013.